Master Thesis

Polarization dependence of X-ray absorption spectra of graphene

Graduate School of Science, Tohoku University
Department of Physics

Mohammed Tareque Chowdhury

2011

Acknowledgements

I would like to thank Prof. Riichiro Saito for his guidance during my two years Master course in physics. He was very patient to teach me physics. I am very grateful to him. I would like to express my gratitude to Dr. Kentaro Sato for many fruitful discussions regarding the formulation of non vertical transition. I am also very much grateful Dr. Alex Gruneis (past member of our group), because his doctor thesis help me to understand the dipole approximation in optical absorption process. I would like to thank Mr. Takahiro Eguchi who was my tutor for first one year. He was a kind person and we often discussed about the progress of our research work. I am very thankful to Dr. Li-Chang Yin, Rihei Endo, Md. Mahbubul Haque, A.R.T Nugraha and P.Y Tapsanit. We spent quite a long time together with discussing physics and playing pingpong at the end of the day. I want to thank Dr. Jin-Sung Park and Dr. Wataru Izumida who have been motivating me to do good research. I am very much grateful to Ms. Wako Yoko and Ms. Setsuko Sumino for their kind help and cooperation in praparing many official documents. I expressed my gratitude to MEXT for providing me scholarship during my Master course. I use this opportunity to thank my family, for their encouragement and support gave me strength and confidence to continue my research work. I dedicate this thesis to my family, especially to my wife Tasneem and my son Yamin.

Contents

Chapter 1

Introduction

Graphene is a two dimensional (2D), single isolated atomic layer of graphite with sp^2 bonded carbon atoms. In this 2D sheet, carbon atoms are densely packed in a honeycomb crystal lattice. The nearest carbon-carbon distance in the graphene sheet is 1.42Å [1]. In the three dimensional (3D) graphite the interlayer seperation is 3.35Å which is large in comparison to the in-plane carbon-carbon distance. Because of this weak interlayer interaction, the energy band structure of 2D graphene is an approximation of 3D graphite. Graphene is a main structural unit of graphite, carbon nanotube, fullerene etc. The band structure of 2D graphene is already known in 1950's [2] but it was long been preassumed that a purely two dimensional single graphitic layer can never exist. However, in 2004, Novoselov *et al.* [3] experimentally discovered the 2D graphene sheet using a simple method called micromechanical cleavage or exfoliation technique. Since then, graphene attracted researchers attention for its many exotic physical properties.

Electronically, graphene is a zero band gap semiconductor because its valence band and conduction band touch each other at the K points (the hexagonal corner) in the Brillouin zone. Therefore the electronic density of states (DOS) at the Fermi level (or charge neutral point) is zero. Due to the linear energy dispersion around the K points, the electrons show zero effective mass and moving at a speed 300 times smaller than the speed of light, that is 10^6m/s. The electron in graphene is thus governed by relativistic Dirac equation. The massless charged particle is called Dirac

Fermion [4]. Dirac Fermion shows anomalous integer quantum Hall effect when it is subject to magnetic field [5, 4]. It is exeperimentally observed that graphene shows very high mobility 300,000cm^2/Vs at room temperature [6]. A single layer graphene absorbs 2.3% of white light which is very high opacity for a single atomic layer [7]. Spin-orbit interaction in graphene is also very weak compared with those for transition metal. Due to such unique properties, graphene is a promising material for future applications in spinotronics, ultrafast photonics and quantum computers, etc.

X-ray absorption spectroscopy(XAS), photoemission spectroscopy(PES), electron energy loss spectroscopy(EELS) are very important methods for characterizing the electronic properties of materials. Especially X-ray absorption spectroscopy which is a core electron exicitation process provides information not only on core-electron energy but also on the unoccupied electronic states in materials. Such states can originate from the bulk properties of materials or due to geometric edge structure (in case of graphene nano-ribbon) or by inclusion of dopant. Characterization of XAS spectral features is essential to confirm the quality of the material before it is ready for application. Recently, several groups have published X-ray absorption spectra of graphene and graphitic materials [8, 9, 10]. R.A Rosenberg *et al.* [8] shows polarization dependence of X-ray absorption spectra of single crystal graphite in which opposite polarization depenence appear for the final states of $\pi^*$and σ^* to each other. Such observed spectral features are relavent to the unoccupied electronic wavefucntion and their symmetry. Gruneis *et al.* [11] and Saito *et al.* [12] explained optical absorption in graphene for π to π^* within the dipole approximation. Such an analytical description is very helpful to understand the absorption process, which we applied to XAS cases.

1.1 Purpose of the study

In this thesis, we discuss (a) why such transitions occur (b) how the polarization directions change the intensity of transitions. Here we adopt an analytical way to answer such questions. The purpose of this thesis is to understand the X-ray absorption spectra using the so-called dipole approximation considering both the on-site and off-

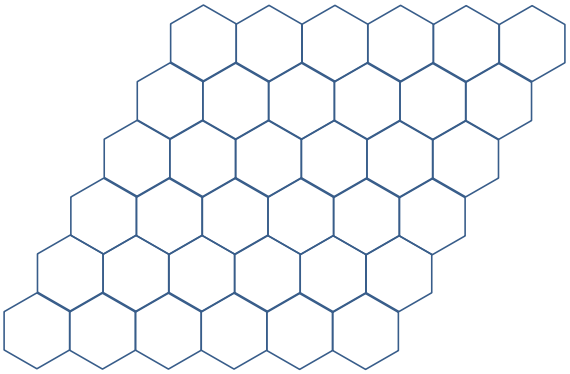

Figure 1-1: Hexagonal honeycomb lattice structure of graphene. Each hexagon corner is a position of a carbon atom. Thus each carbon atom make sigma bond with three nearest neighbor carbon atom and created this hexagonal lattice structure.

site transitions which was discussed by Gruneis *et al.* [11] for $\pi - \pi^*$ and then to find an answer of how the polarization direction changes the X-ray absorption intensity.

1.2 Background

Hereafter in this chapter, we discuss the background for the present thesis.

1.2.1 Atomic bonding in graphene

In graphene, the electronic bond nature of carbon atoms can be described by the so-called sp^2 hybridization. There are three sp^2 hybrid orbitals in each carbon atom formed by the mixing of 2s, $2p_x$ and $2p_y$ orbitals to one another. These three in-plane σ bonds pointing in the in-plane nearest neighbour atoms are responsible for the hexagonal crystal structure of graphene as shown in Fig. 1-1. The fourth electron lies in the $2p_z$ orbital, which is oriented perpendicular to σ bond plane and form a weaker π bond. The π electrons which are valence electrons are responsible for the electronic transport properties of graphene.

Fig. 1-1: figure/hexlatt.pdf

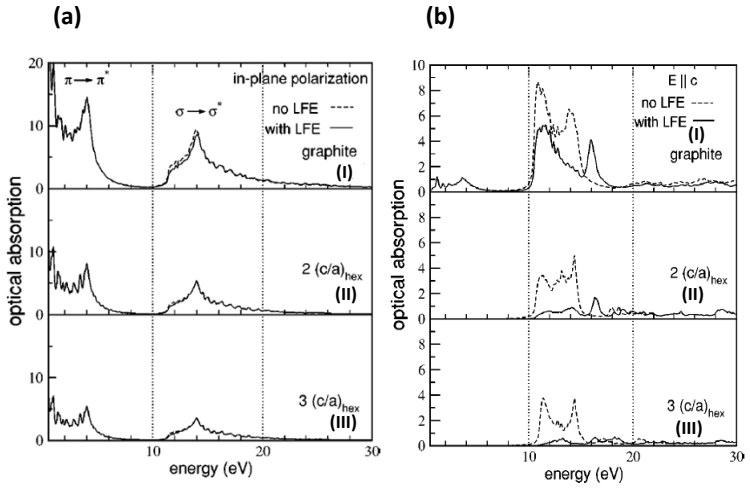

Figure 1-2: (a) Optical absorption spectrum of (I)graphite and graphene sheet geometries with (II) $2(\frac{c}{a})_{hex}$ and (III)$3(\frac{c}{a})_{hex}$ for $\vec{E} \perp \vec{c}$. The spectrum is displayed with broadening of 0.1eV (b) Optical absorption spectrum of (I)graphite and graphene sheet geometries with (II)$2(\frac{c}{a})_{hex}$ and (III) $3(\frac{c}{a})_{hex}$ for $\vec{E} \parallel \vec{c}$. (reproduced from Fig.4 and Fig.5 of ref [15]).

1.2.2 Spectroscopic methods for graphene

Optical absorption Spectroscopy

When visible light with 1 eV to 3 eV energy allow to passes through a solid, some photons with particular energy and wavelength can be absorbed. Quantum mechanically, electrons can be excited from occupied valence band to unoccupied conduction band. Such absorption intensity can vary as a function of energy which is well-described by the joint density of states(JDOS) [13]. The absorption spectra provide useful information about the electronic structure of materials. The interband contribution to the frequency-dependent dielectric constant for graphite was calculated for both parallel and vertical polarization by Jonson *et al.* [14]. An *ab-initio* calculation of the optical absorption spectra of graphite and graphene sheets was calculated by Marinopoulos *et al.* [15] which is shown in Fig. 1-2.

They identified the interband transitions that are responsible for the most promi-

Fig. 1-2: figure/marinopolous_opt.pdf

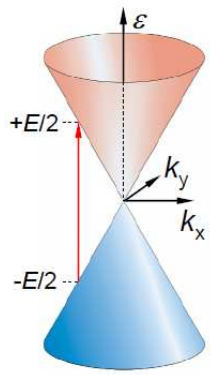

Figure 1-3: Excitation process responsibe for absorption of light in graphene. Electrons from the valence band (blue) are excited to the empty states in the conduction band (red) with conserving their momentum and gaining energy $E = \hbar\omega$. (reproduced from Fig.S5 of ref [7]).

nent peak in the absorption spectra. Generally, optical transitions occur vertically in the k-space, because such a low energy photon contributes negligible momentum to that for an electron in solids and thus the electrons are excited from the valence to the conduction bands with the same wave vectors $\vec{k}$ in the first Brillouin zone. This optical transition process in graphene around K points can be shown in Fig. 1-3 .

Usually, the optical absorpton intensity is expressed as a function of energy. This is because the absorption intensity is contributed by all possible k points in the Brillouin zone. Optical absorption in graphene corresponds to π-π^* transition in the 2D graphite or graphene. A. Gruneis *et al.* [11] calculated optical absorption of graphite and carbon nanotube using the so-called dipole approximation in which the absoprtion amplitude is proportional to $\vec{P} \cdot \vec{D}$. The iner product of the polarization of light P and the dipole vector $\langle \Psi^f \mid \nabla \mid \Psi^i \rangle = \vec{D}$. Fig. 1-4 shows a node of intensity in an equi energy circle around K points in the Brillouin zone when a particular energy and polarization is selected, where the highlighted line corresponds to k-vectors which gives strong photoluminescence (PL) intensity. The reason of such a node being observed in the Brillouin zone is that the energy dispersion in graphene is linear near the K points. In most materials the quadratic terms in k_x and k_y appear around the energy bottom of the energy band, and hence such a node does not exist.

Fig. 1-3: figure/ohta_science_opt.pdf

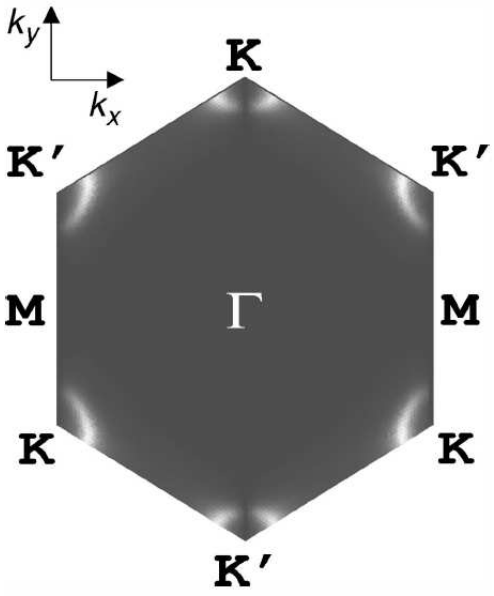

Figure 1-4: Plot of optical absorption intensity $W(k)$ over the 2D Brilloun zone of graphite. The polarization vector and the laser energy are selected as $P(0,1)$ and $E_{laser} = 3$eV, respectively. It can be seen that the absorption is zero along the horizontal lines connecting the K and K' points. (reproduced from Fig. 1 of Ref. [11]).

(a)The energy dispesion relation of π and σ bands of 2D graphene along the high symmetry direction, (b)The joint density of states (JDOS) of graphene as a function of energy. The JDOS is corresponds to the X-ray absorption. Electron is excited from the 1s orbitals

X-ray absorption spectroscopy(XAS)

Next let us discuss about the X-ray absorption spectroscopy (XAS). When X-ray is incident on a material, the X-ray photons excite the core electrons ($1s$, $2s$ etc) to the unoccupied states above the Fermi level. At a certain energy around 285eV 290eV, the absorption increase drastically and give rise to an absorption edge that occurs when the incident photon energy is just sufficient to cause excitation of a 1s electron to the unoccupied states. Generally, if an electron is excited from the 1s then it is called the K-edge absorption. X-ray absorption spectra provide information about the DOS of unoccupied states since DOS of 1s energy band has a small band width.

Fig. 1-4: figure/gruneis_opt.pdf

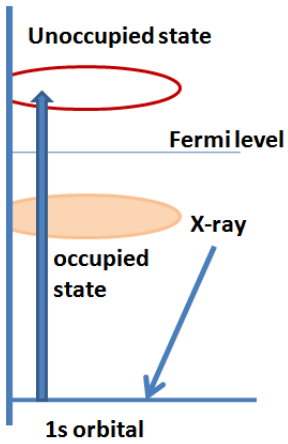

Figure 1-5: Schematic picture of X-ray absorption process.

Fig. 1-5 shows the schematic of X-ray absorption process.

Experimental observations of X-ray absorption fine structure (XAFS) of graphite were done by many different groups [8, 16, 17, 18]. Rosenberg *et al.* [8] found important informaton regarding the angular dependence of the intensity. The spectra for single crystal graphite shows that the intensity changes as a fucntion of α the angle between the Poynting vector and the surface normal. At the same time the final state symmetry can be selected by varying the angle of polarization direction as shown in Fig. 1-6. That is the intensity of 1s to π^* transition is proportional to $\sin^2\alpha$ and while the intensity of a 1s to σ^* transition is proportional to $\cos^2\alpha$.

Recently, some researchers experimentally observed the X-ray absorption spectra of a 2D monolayer and few layer graphene [10, 9]. Fig. 1-7 shows C K absorption spectra obtained for graphene, bilayer graphene and few layer graphene sample. The peak at 285.5eV is associated with π^* transition while the σ^* states appear at 291.5 eV. A sharp peak (weak) of the 1s to π^* (σ^*) transition is observed because polarization direction was almost perpendicular to the basal plane of graphene which is consistent with Rosenberg *et al.* [8]. There are two contribution to the XAS intensity, (1) the matrix element between initial and final states, and (2)the JDOS calculated from the energy band structure. Such an enhancement or de-enhancement of the transition

Fig. 1-5: figure/xas_intro.pdf
Fig. 1-6: figure/rosenberg_xas.pdf

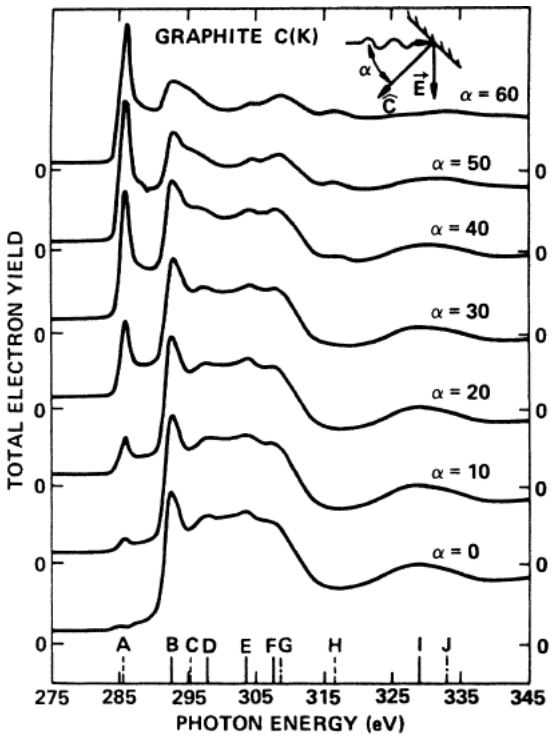

Figure 1-6: C(K)-edge absorption spectra of single-crystal graphite at various polarization angle α between the surface normal and the Poynting vector of the light. Lines at the bottom of the figure are lines showing the peak energies: dashed lines represent the states of π^* symmetry, while solid lines represent the states of σ^* symmetry. States whose symmetry could not be determined are represented by dashed dotted lines. The monochromatic photon energy calibration is estimated to be accurate to $\pm 0.5eV$. (reproduced from Fig. 1 of Ref. [8]).

intensity may be the the effect of polarization dependence of matrix element.

Zhou *et al.* [9] also show XAS spectra of single layer exfoliated graphene on two different polarizations. It is shown in Fig. 1-8 that when the light polarization lies within plane, only the in-plane σ^* orbital contributes to the C 1s edge at 292eV while when the out-of-plane polarization component increases the intensity of the π^* feature at 285eV strongly increases. This polarization dependence confirms the in-plane and out-of-plane character of σ^* and π^* orbitals.

Recently Weijie Hua *et al.* [19] calculated XAS of graphene using first principle calculation. The infinite graphene sheet is simulated different width of graphene

Fig. 1-7: figure/pachile_xas.pdf
Fig. 1-8: fig/zhou_xas.pdf

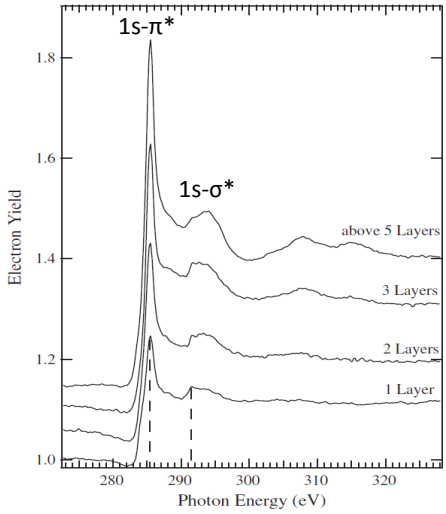

Figure 1-7: C *K*-edge photo absorption spectra of (from the bottom): graphene ,bylayer graphene, and FLG sample. The dased lines show the C 1s π^* and C 1s σ^* transition. (reproduce from Fig. 2 of Ref. [10]).

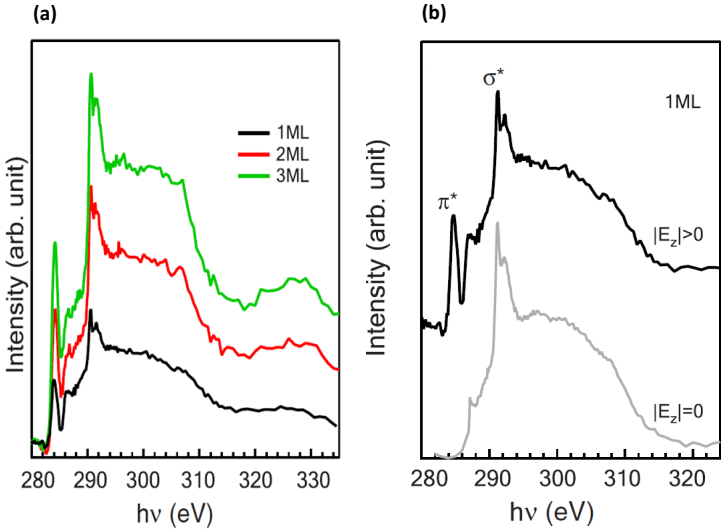

Figure 1-8: (a)C 1s spectra taken on single layer exfoliated grapehene with zero (white curve) and nonzero (black curve) out-of-plane polarization component EZ respectively (b) C 1s spectra taken from monolayer, bilayer, and trilayer graphene with nonzero out-of-plane polarization. (reproduced from fig 1(c)and 1(d) of Ref. [9]).

nanoribbon. Using such a calculation they analyzed the effect of edge, defect or stacking on the characteristic XAS. An ideal 2D infinite graphene plane has one unique π^* peak. But in the real case due to the presence of edges, defect or broken

periodic symmetry can create more features in th XAS. From these spectral feature, interpretation can be made on graphene in the different conditions.

Electron energy loss spectroscopy(EELS)

Although we do not calculate, we briefly describe EELS since EELS is an alternative spectrocopy for unoccupied states. Elecetron energy loss spectroscopy (EELS) is based on the analysis of energy loss of incident electron by the interaction with a material. If an electron is incident on a material, because of the inelastic scattering, the incoming electron loses some part of its energy to the target atom. Such an energy loss can be very small (less than 0.1eV) which corresponds to excitation of lattice vibration of atoms on a clean surface. When energy losses are within a few eV, excitations of transition originating from the valence band (interband and intraband transition, surface states, etc.) will occur. The core level excitation occurs when such energy loss is a few hundreds of electron volts. This is called high energy electron loss spectroscopy (HEELS). This core excitation process is similar to that of XAS feature. Fig. 1-9 shows both XAS and EELS processes.

In the X-ray absorption process, the resonance condition is satisfied when the incident photon energy is equal to the energy difference between the initial state and final unoccupied state. In the HEELS process, the number of scattered electron of the beam was counted. Since this electron excited the core electron to the same final states as of X-ray absorption, if the incoming electron energy is much larger than that of the bound electron, then the incoming and outgoing electron can be expressed by the plane waves. In such a case we can write the expression for the distribution of electron yield distribution N(E)within the dipole approximation as,

$$N(E) = \frac{d\sigma}{dq} \propto \frac{1}{q} \mid \langle \Psi_f \mid \vec{\epsilon_q} \cdot \vec{r_a} \mid \Psi_i \rangle \mid^2, \tag{1.1}$$

where $\vec{q}$ is momentum, σ is the differential scattering cross section of the momentum transfer, Ψ_f and Ψ_i is the final and initial states of the core electron, ϵ is the unit

Fig. 1-9: figure/carcucci_eels.pdf

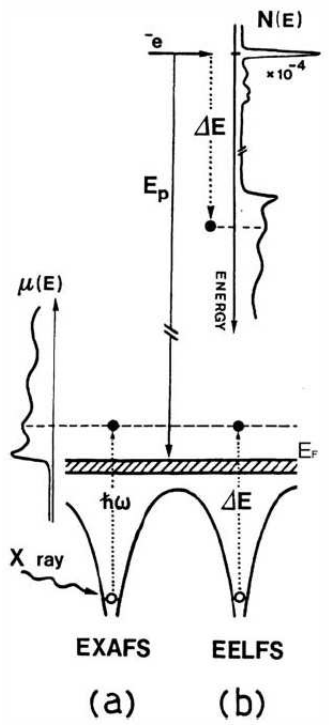

Figure 1-9: Fine structures(FS) of (a) XAS and (b) EELS spectroscopies. (reproduced from Fig. 8 of Ref. [20] and Ref. [21]).

vector in the direction of $\vec{q}$ vector and $\vec{r_a}$ is the atomic radius of the core electron.

This expression is similar to the X-absorption intensity $\mu(E)$,

$$\mu(E) \propto | \langle \Psi_f(\vec{k}) \mid \vec{\epsilon} \cdot \vec{r_a} \mid \Psi_i \rangle |^2, \tag{1.2}$$

where $\vec{\epsilon}$ is the unit vector of the electric field in the direction of the X-ray polarizaton.

Angle resolved Photoemission Spectroscopy(ARPES)

Angle resolved photo emission spectroscopy (ARPES) is related to the photoelectron emission process where the photo excited electron is emitted from a material by the interaction with a monochromatic light. Fig. 1-10 shows the photoemission process of ARPES. The kinetic energy of the emitted electron can be written in a simple expression given by Einstein (1905) as

$$E_{\text{kin}} = hf - \phi - \mid E_b \mid . \tag{1.3}$$

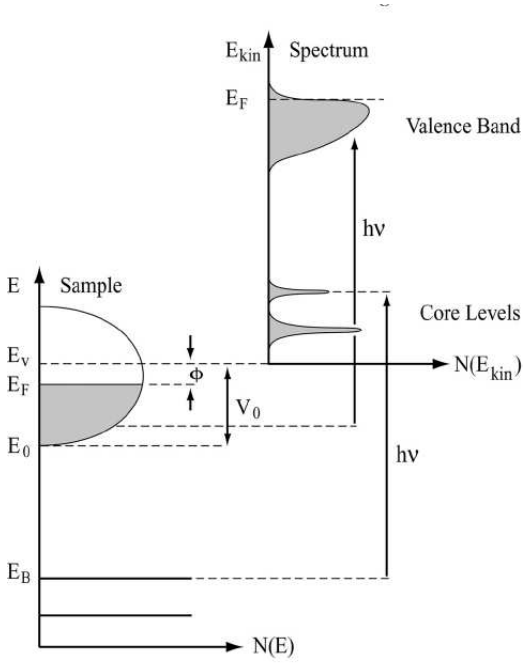

Figure 1-10: Energetics of the photoemission process. The electron energy distribution, $N(E_{\rm kin})$, are produced for valence band or core levels by the incoming photons and measured as a function of kinetic energy $E_{\rm kin}$ of the photo-electron. $N(E_{\rm kin})$ is expressed in terms of the binding energy E_b(left) and work funtion ϕ and $\hbar f$.(reproduced from Ref. [22]).

where $E_{\rm kin}$ is the kinetic energy of the photoelectron. h is the Planck constant and f is the frequency of the incident mochromatic photon, ϕ is the work function. $|E_b|$ is the electron binding energy in the solid.

When a beam of monochromatic light incident on the sample, electrons are emitted as a result of the photoelectric effect. These emitted electrons are collected by electron analyzer. This electron analyzer can measure the electron kinectic energy $E_{\rm kin}$ at some emission angles. In this way the photolectron momentum can be measured. As the total energy and the momentum of the electron and photon is conserved before and after scattering, we can relate the photo electron kinetic energy and the momentum with electron binding energy inside solid and the crystal momentum. In this way, the occupied electronic band strucure can be directly observed by ARPES experiment.

Bostwick *et al.* [23] experimentally observed the band structure of graphene which

Fig. 1-10: figure/damas_arpes.pdf

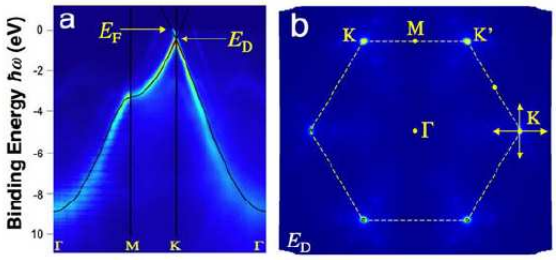

Figure 1-11: The π band structure of graphene. (a) The experimental energy distribution of states as a function of momentum along the high symmetry line with a single orbital model (solid lines) given by Eq. (1.4).(b) Constant energy map of the states at binding energy corresponding to the Dirac energy (E_D) together with the Brillouin zone boundary(dashed line). (reproduced from Figs. 1(a) and 1(b) of Ref. [23]).

is shown in Fig. 1-11. In this experiment a single layer of graphene is grown on the surface of SiC(6H polytype). This observation shown in Fig. 1-11 is comparable with the two dimensional π band structure of graphene can be expressed as

$$E(\vec{k}) = \pm t\sqrt{1 + 4\cos\frac{\sqrt{3}k_y a}{2}\cos\frac{k_x a}{2} + 4\cos^2\frac{k_x a}{2}} \tag{1.4}$$

where $\vec{k}$ is the in-plane momentum, a is the lattice constant, and t < 0 is the nearest neighbor hopping energy.

A theoretical treatment for photoexcitation process of single crystal graphite in ARPES is given by Shirley *et al.* [24]. In this picture, the initial state wave function is atomic like orbital and the final state wave function can be described by a form of plane wave. In this thesis, we follow this treatment and try to calculate for some reciprocal lattice vector $\vec{G}$.

1.3 Organization

This thesis is organised into five chapters. Chapter 1 includes introduction and all necessary background. In Chapter 2 we describe the electronic structure of graphene, starting from its unit cell and reciprocal lattice. We formulate the tight binding model

Fig. 1-11: figure/bostwick1_arpes.pdf

which is employed to calculate the π^* and σ^* band within nearest neighbour approximation. The so-called dipole approximation is reviewed in this chapter following the previous work of Gruneis *et al.* [11]. However, we discuss the dipole approximation for X-ray absorption process where the optical transition cannot be treated as vertical transition. Atomic matrix elements for the on-site and off-site transitions are discussed in this chapter. Gaussian type lineshapes are used to simulate atomic orbitals, and then the analytical expression for on-site and the off-site transition matrix elements are derived. In Chapter 3, the original calculated results of this thesis are shown. In Chapter 4, a summary and conclusions of the present thesis are given.

Chapter 2

Calculation method

The basic properties of graphene are reviewed in this chapter. The discussion includes a description of the graphene geometrical structure and electronic properties. The electronic structure calculation is within the tight-binding framework. Then, we show how to calculate X-ray absorption intensity as a function of wave vector $\vec{k}$ for the final electronic states and as a function of X-ray energy using dipole approximation.

2.1 Geometrical structure of graphene

2.1.1 Graphene unit cell

Graphene is a single atomic layer of carbon atoms in a 2D honeycomb lattice. Graphene is basic building block for all graphitic materials of other dimension. Several layers of graphene sheet are stacked togather will form 3D graphite, where the carbon atoms in each of the 2D layer make strong sp^2 bonds and the van der Waals forces describe a weak interlayer coupling. Fig. 2-1(a) and (b) give the unit cell and Brillouin zone of graphene respectively. The graphene sheet is generated from the dotted rhombus unit cell shown by the lattice vectors $\vec{a_1}$ and $\vec{a_2}$, which are defined as.

$$\vec{a_1} = a\left(\frac{\sqrt{3}}{2}, \frac{1}{2}\right), \quad \vec{a_2} = a\left(\frac{\sqrt{3}}{2}, -\frac{1}{2}\right), \tag{2.1}$$

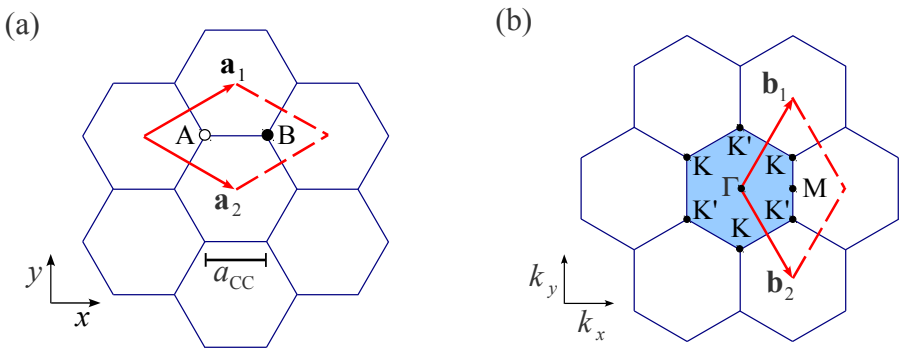

Figure 2-1: (a) Unit cell and (b) the Brillouin zone of graphene are shown, respectively, as the dotted rhombus and the shaded hexagon. $\vec{a}_i$ and $\vec{b}_i$, $(i = 1, 2)$ are unit vectors and reciprocal lattice vectors, respectively. The unit cell in real space contains two carbon atoms A and B. The dots labeled Γ, K, K', and M in the Brillouin zone indicate the high-symmetry points.

where $a = \sqrt{3}a_{cc} = 2.46$Å is the lattice constant for the graphene sheet and $a_{cc} \approx 1.42$Å is the nearest-neighbor interatomic distance. The unit cell consists of two distinct A, B carbon atoms which form the A and B sublattices, respectively, by open and solid dots shown in Fig. 2-1(a). The reciprocal lattice vectors $\vec{b_1}$ and $\vec{b_2}$ are related to the real lattice vectors $\vec{a_1}$ and $\vec{a_2}$ according to the definition

$$\vec{a_i} \cdot \vec{b_j} = 2\pi\delta_{ij}, \tag{2.2}$$

where δ_{ij} is the Kronecker delta, so that $\vec{b_1}$ and $\vec{b_2}$ are given by

$$\vec{b_1} = \frac{2\pi}{a}\left(\frac{1}{\sqrt{3}}, 1\right), \quad \vec{b_2} = \frac{2\pi}{a}\left(\frac{1}{\sqrt{3}}, -1\right). \tag{2.3}$$

The first Brillouin zone is shown as a shaded hexagon in Fig. (2-1)(b), where Γ, K, K', and M denote the high symmetry points.

2.2 Tight-binding framework

In this section, we will describe the simple tight binding model for 2D graphene. The electronic dispersion relations of a graphene sheet are obtained by solving the single

Fig. 2-1: fig/fch2-grunit.pdf

particle Schrödinger equation:

$$\hat{H}\Psi^b(\vec{k},\vec{r}) = E^b\Psi^b(\vec{k},\vec{r}), \tag{2.4}$$

where $\hat{H}$ is the Hamiltonian, and E^b and Ψ^b are, respectively eigen energy and wave fucntion with band index b. $\hat{H}$ is given by

$$\hat{H} = -\frac{\hbar^2}{2m}\nabla^2 + U(\vec{r}). \tag{2.5}$$

where ∇ is the gradient operator, $\hbar$ is the Plank's constant, m is the electron mass, the first term is the kinetic energy operator, $U(\vec{r})$ is the effective periodic potential. The electron wavefunction $\Psi^b(\vec{k},\vec{r})$ is approximated by a linear combination of the Bloch functions:

$$\Psi^b(\vec{k},\vec{r}) = \sum_{s}^{A,B}\sum_{o}^{2\mathrm{s},\ldots,2\mathrm{p_z}} C^b_{so}(\vec{k})\Phi_{so}(\vec{k},\vec{r}), \tag{2.6}$$

where $E^b(\vec{k})$ is the one-electron energy, $C^b_{so}(\vec{k})$ is the coefficient to be solved, $\Phi_{so}(\vec{k},\vec{r})$ is the Bloch wavefunction which is given by sum over A and B atom and the atomic orbital wave functions $\phi_o(\vec{r})$ at each orbital at the u-th unit cell in a graphene sheet.

$$\Phi_{so}(\vec{k},\vec{r}) = \frac{1}{\sqrt{U}}\sum_{u}^{U} e^{i\vec{k}.\vec{R}_{us}}\phi_o(\vec{r}-\vec{R}_{us}), \tag{2.7}$$

The index $u = 1,..,U$ goes over all the U unit cells in a graphene sheet and $\vec{R}_{us}$ is the atomic coordinate for the u-th unit cell and s-th atom, o represents the 2s, $2\mathrm{p_x}$, $2\mathrm{p_y}$ and $2\mathrm{p_z}$ orbital of carbon atom. The eigenvalue $E^b(\vec{k})$ as a function of $\vec{k}$ is given by

$$E^b(\vec{k}) = \frac{\langle\Psi^b(\vec{k}) \mid H \mid \Psi^b(\vec{k})\rangle}{\langle\Psi^b(\vec{k}) \mid \Psi^b(\vec{k})\rangle}. \tag{2.8}$$

putting the value of $\Psi^b(\vec{k},\vec{r},t)$ in Eq. (2.8), we get

$$E^b(\vec{k}) = \frac{\sum_{s'o'}\sum_{so} C^{b*}_{s'o'}(\vec{k})H_{s'o'so}(\vec{k})C^b_{so}(\vec{k})}{\sum_{s'o'}\sum_{so} C^{b*}_{s'o'}(\vec{k})S_{s'o'so}(\vec{k})C^b_{so}(\vec{k}}), \tag{2.9}$$

The transfer integral $H_{s'o'so}(\vec{k})$ and the overlap integral $S_{s'o'so}(\vec{k})$ can be defined as

$$H_{s'o'so}(\vec{k}) = \frac{1}{U}\sum_{u}^{U} e^{i\vec{k}\cdot(\vec{R}_{us}-\vec{R}_{u's'})}\int \phi^*_{o'}(\vec{r}-\vec{R}_{u'A'})H\phi_o(\vec{r}-\vec{R}_{us})d\vec{r}, \tag{2.10}$$

$$S_{s'o'so}(\vec{k}) = \frac{1}{U}\sum_{u}^{U} e^{i\vec{k}\cdot(\vec{R}_{uB}-\vec{R}_{u's'})}\int \phi^*_{o'}(\vec{r}-\vec{R}_{u'A})\phi_o(\vec{r}-\vec{R}_{us})d\vec{r}. \tag{2.11}$$

The variational condition for finding the minimum of the ground state energy is

$$\frac{\partial E^b(\vec{k})}{\partial C^{b*}_{s'o'}(\vec{k})} = 0. \qquad (s = A, B, o = 2\mathrm{s}, 2\mathrm{p_x}, 2\mathrm{p_y}, 2\mathrm{p_z}) \tag{2.12}$$

Differentiating Eq. (2.9) we get,

$$\begin{aligned}
\frac{\partial E^b(\vec{k})}{\partial C^{b*}_{s'o'}(\vec{k})} =& \frac{\sum_{so} H_{s'o'so}(\vec{k})C^b_{so}(\vec{k})}{\sum_{s'o'}\sum_{so} C^{b*}_{s'o'}(\vec{k})S_{s'o'so}(\vec{k})C^b_{so}(\vec{k})} \\
&- \frac{\sum_{s'o'}\sum_{so} C^{b*}_{s'o'}(\vec{k})H_{s'o'so}(\vec{k})C^b_{so}(\vec{k})}{(\sum_{s'o'}\sum_{so} C^{b*}_{s'o'}(\vec{k})S_{s'o'so}(\vec{k})C^b_{so}(\vec{k}))^2}\sum_{so} S_{s'o'so}(\vec{k})C^b_{so}(\vec{k}) \\
=& \frac{\sum_{so} H_{s'o'so}(\vec{k})C^b_{so}(\vec{k}) - E^b(\vec{k})\sum_{so}\sum_{so} S_{s'o'so}(\vec{k})C^b_{so}(\vec{k})}{\sum_{s'o'}\sum_{so} C^{b*}_{s'o'}(\vec{k})S_{s'o'so}(\vec{k})C^b_{so}(\vec{k})} \\
=& 0,
\end{aligned}$$

which gives the simultaneous eight equations,

$$\sum_{so} H_{s'o'so}(\vec{k})C^b_{so}(\vec{k}) - E^b(\vec{k})\sum_{so} S_{s'o'so}(\vec{k})C^b_{so}(\vec{k}) = 0. \quad (s' = A, B.o' = 2\mathrm{s}, 2\mathrm{p_x}, 2\mathrm{p_y}, 2\mathrm{p_z}) \tag{2.13}$$

Eq. (2.13) is expressed by a matrix form when we define the $C^b_{so}(\vec{k})$ as a column vector,

$$(H(\vec{k}) - E^b(\vec{k})S(\vec{k}))C^b(\vec{k}) = 0, \qquad (b = 1, .., 8),$$

$$C^b(\vec{k}) = \begin{pmatrix} C^b_{2\mathrm{s^A}} \\ \vdots \\ C^b_{2\mathrm{pz^B}} \end{pmatrix} \tag{2.14}$$

The eigen values of $H_{s'o'so}(\vec{k})$ are calculated by solving the following secular equation for each $\vec{k}$,

$$\det[H(\vec{k}) - E^b(\vec{k})S(\vec{k})] = 0. \tag{2.15}$$

This Eq. (2.15) gives eight eigen values of $E^b(\vec{k})$ for the energy band index b,$(b = 1, ..., 8)$ for a given electron wave vector $\vec{k}$. We have four atomic orbitals 2s, $2\mathrm{p_x}$, $2\mathrm{p_y}$ and $2\mathrm{p_z}$ at each atom. Then 8×8 Hamiltonian and overlap matrix can be expressed by 2×2 submatrix for two atoms.

$$H(\vec{k}) = \begin{pmatrix} H_{AA}(\vec{k}) & H_{AB}(\vec{k}) \\ H_{BA}(\vec{k}) & H_{BB}(\vec{k}) \end{pmatrix}, \tag{2.16}$$

and S is simply expressed as

$$S(\vec{k}) = \begin{pmatrix} S_{AA}(\vec{k}) & S_{AB}(\vec{k}) \\ S_{BA}(\vec{k}) & S_{BB}(\vec{k}) \end{pmatrix}, \tag{2.17}$$

where $H_{AA}(H_{BB})$ and $H_{AB}(H_{BA})$ are 4×4 submatrix for the four orbitals. The matrix element between $2\mathrm{p_z}$ orbital and $2\mathrm{s}, 2\mathrm{p_x}$ and $2\mathrm{p_y}$ are zero because of the odd

(even) function $2p_z(2s, 2p_x$, and $2p_y)$ of z for the both cases of $H_{AA}(H_{BB})$;

$$
\begin{aligned}
H_{AA}(\vec{k}) &= \begin{pmatrix}
\langle 2s^A \mid H \mid 2s^A \rangle & \langle 2s^A \mid H \mid 2p_x^A \rangle & \langle 2s^A \mid H \mid 2p_y^A \rangle & \langle 2s^A \mid H \mid 2p_z^A \rangle \\
\langle 2p_x^A \mid H \mid 2s^A \rangle & \langle 2p_x^A \mid H \mid 2p_x^A \rangle & \langle 2p_x^A \mid H \mid 2p_y^A \rangle & \langle 2p_x^A \mid H \mid 2p_z^A \rangle \\
\langle 2p_y^A \mid H \mid 2s^A \rangle & \langle 2p_y^A \mid H \mid 2p_x^A \rangle & \langle 2p_y^A \mid H \mid 2p_y^A \rangle & \langle 2p_y^A \mid H \mid 2p_z^A \rangle \\
\langle 2p_z^A \mid H \mid 2s^A \rangle & \langle 2p_z^A \mid H \mid 2p_x^A \rangle & \langle 2p_z^A \mid H \mid 2p_y^A \rangle & \langle 2p_z^A \mid H \mid 2p_z^A \rangle
\end{pmatrix} \\
&= \begin{pmatrix}
\langle 2s^A \mid H \mid 2s^A \rangle & 0 & 0 & 0 \\
0 & \langle 2p_x^A \mid H \mid 2p_x^A \rangle & 0 & 0 \\
0 & 0 & \langle 2p_y^A \mid H \mid 2p_y^A \rangle & 0 \\
0 & 0 & 0 & \langle 2p_z^A \mid H \mid 2p_z^A \rangle
\end{pmatrix} \\
&= H_{BB}(\vec{k}),
\end{aligned} \tag{2.18}
$$

and,

$$
\begin{aligned}
H_{AB}(\vec{k}) &= \begin{pmatrix}
\langle 2s^A \mid H \mid 2s^B \rangle & \langle 2s^A \mid H \mid 2p_x^B \rangle & \langle 2s^A \mid \mathrm{H} \mid 2p_y^B \rangle & \langle 2s^A \mid H \mid 2p_z^B \rangle \\
\langle 2p_x^A \mid H \mid 2s^B \rangle & \langle 2p_x^A \mid H \mid 2p_x^B \rangle & \langle 2p_x^A \mid H \mid 2p_y^B \rangle & \langle 2p_x^A \mid H \mid 2p_z^B \rangle \\
\langle 2p_y^A \mid H \mid 2s^A \rangle & \langle 2p_y^A \mid H \mid 2p_x^A \rangle & \langle 2p_y^A \mid H \mid 2p_y^B \rangle & \langle 2p_y^A \mid H \mid 2p_z^B \rangle \\
\langle 2p_z^A \mid H \mid 2s^A \rangle & \langle 2p_z^A \mid H \mid 2p_x^B \rangle & \langle 2p_z^A \mid H \mid 2p_y^B \rangle & \langle 2p_z^A \mid H \mid 2p_z^B \rangle
\end{pmatrix} \\
H_{AB}(\vec{k}) &= \begin{pmatrix}
\langle 2s^A \mid H \mid 2s^B \rangle & \langle 2s^A \mid H \mid 2px^B \rangle & \langle 2s^A \mid H \mid 2p_y^B \rangle & 0 \\
\langle 2p_x^A \mid H \mid 2s^B \rangle & \langle 2p_x^A \mid H \mid 2px^B \rangle & \langle 2p_x^A \mid H \mid 2p_y^B \rangle & 0 \\
\langle 2p_y^A \mid H \mid 2s^A \rangle & \langle 2p_y^A \mid H \mid 2px^A \rangle & \langle 2p_y^A \mid H \mid 2p_y^B \rangle & 0 \\
0 & 0 & 0 & \langle 2p_z^A \mid H \mid 2p_z^B \rangle
\end{pmatrix} \\
&= H_{BA}^*(\vec{k})
\end{aligned} \tag{2.19}
$$

We can now calculate the π band and σ band independently by splitting the 8×8 matrix in to 2×2 and 6×6 matrix, because the π orbital is directed along the perpendicular direction of the graphene plane and σ orbitals are lie along the graphene plane, and thus there is no interaction between π and σ orbitals as is shown in Eq. (2.18) and Eq. (2.19).

2.2.1 π band of two dimensional graphene

The simple tight binding model (STB) model, there are three parameters, the atomic orbital energy ϵ_{2p}, the transfer integral $t_{\pi\pi}$, and the overlap integral $s_{\pi\pi}$. Herafter transfer and overlap integrals will simply be t, and s respectively. To construct the 2×2 hamiltonian and overlap matrices, we consider the nearest-neighbor interactions ($R = a_{\rm cc}$) in the unit cell of a graphene sheet. The unit cell contains two atoms, A and B, each of which has three nearest neighbors of the opposite atom type. The absence of nearest-neighbor interactions within the same A or B sublattice gives the diagonal Hamiltonian and overlap matrix elements, $H_{AA} = H_{BB} = \epsilon_{2p}$ and $S_{AA} = S_{BB} = 1$;

$$\begin{aligned} H_{AA}(\vec{k}) &= \frac{1}{U}\sum_{u}^{U} e^{i\vec{k}\cdot(\vec{R}_{uA}-\vec{R}_{u'A})} \int \phi_\pi^*(\vec{r}-\vec{R}_{u'A}) H \phi_\pi(\vec{r}-\vec{R}_{uA}) d\vec{r} \\ &= \frac{1}{U}\sum_{u=u'}^{U} \epsilon_{2p} + \frac{1}{U}\sum_{R_{uA}=R_{u'A}\pm a}^{U} e^{\pm ika} \int \phi_\pi^*(\vec{r}-\vec{R}_{u'A}) H \phi_\pi(\vec{r}-\vec{R}_{u'A}) d\vec{r} \\ &= \epsilon_{2p}, \end{aligned} \tag{2.20}$$

$$\begin{aligned} S_{AA}(\vec{k}) &= \frac{1}{U}\sum_{u}^{U} e^{i\vec{k}\cdot(\vec{R}_{uA}-\vec{R}_{u'A})} \int \phi_\pi^*(\vec{r}-\vec{R}_{u'A}) \phi_\pi(\vec{r}-\vec{R}_{uA}) d\vec{r} \\ &= \frac{1}{U}\sum_{u=u'}^{U} \epsilon_{2p} + \frac{1}{U}\sum_{R_{uA}=R_{u'A}\pm a}^{U} e^{\pm ika} \int \phi_\pi^*(\vec{r}-\vec{R}_{u'A}) \phi_\pi(\vec{r}-\vec{R}_{u'A}) d\vec{r} \\ &= 1. \end{aligned} \tag{2.21}$$

For the off-diagonal matrix element H_{AB}, we consider three nearest neigbor B atoms from the A atom denoted by a vector $\vec{r_A^1}, \vec{r_A^2}$, and $\vec{r_A^3}$.

$$\vec{r_A^1} = \left(\frac{1}{\sqrt{3}}, 0\right) a, \quad \vec{r_A^2} = \left(-\frac{1}{2\sqrt{3}}, \frac{1}{2}\right) a, \quad \vec{r_A^3} = \left(-\frac{1}{2\sqrt{3}}, -\frac{1}{2}\right) a. \tag{2.22}$$

Fig. 2-2 shows the vector connecting three nearest neighbor atoms from center atom.

Putting this value in Eq. (2.11), we can calculate the off-diagonal Hamiltonian

Fig. 2-2: figure/neibor3.pdf

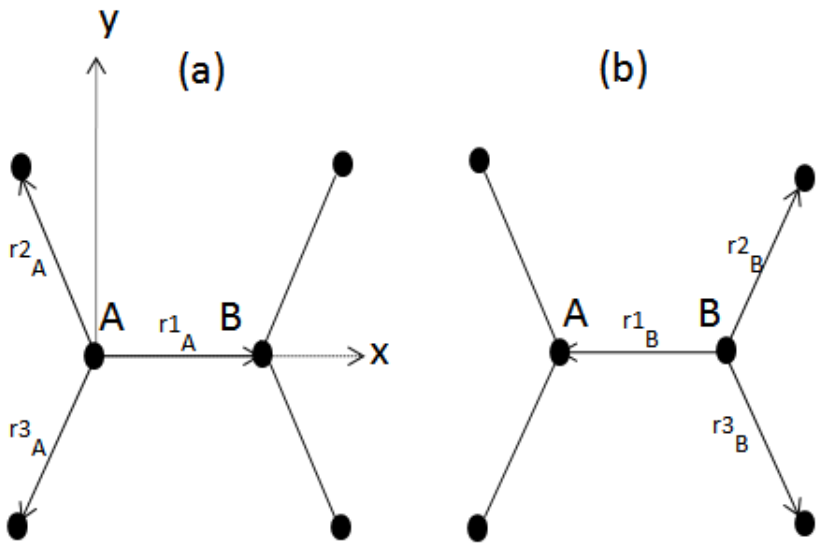

Figure 2-2: Vectors conneting nearest neighbor atoms in graphene for (a) the A atom and (b) the B atom. vectors are given in Eq. (2.22).

matrix element as,

$$\begin{aligned} H_{AB}(\vec{k}) &= \frac{1}{U}\sum_{u}^{U} e^{i\vec{k}\cdot(\vec{R}_{uB}-\vec{R}_{u'A})} \int \phi_{\pi}^{*}(\vec{r}-\vec{R}_{u'A}) H \phi_{\pi}(\vec{r}-\vec{R}_{uB}) d\vec{r} \\ &= t\sum_{n}^{3} e^{i\vec{k}\cdot\vec{r}_{A}^{n}} \\ &= t f(\vec{k}), \end{aligned} \tag{2.23}$$

and the off-diagonal overlap matrix element as,

$$\begin{aligned} S_{AB}(\vec{k}) &= \frac{1}{U}\sum_{u}^{U} e^{i\vec{k}\cdot(\vec{R}_{uB}-\vec{R}_{u'A})} \int \phi_{\pi}^{*}(\vec{r}-\vec{R}_{u'A}) \phi_{\pi}(\vec{r}-\vec{R}_{uB}) d\vec{r} \\ &= s\sum_{n}^{3} e^{i\vec{k}\cdot\vec{r}_{A}^{n}} \\ &= s f(\vec{k}), \end{aligned} \tag{2.24}$$

where t is the transfer integral, s is the overlap integral between the nearest neighbor A and B atoms, and $f(\vec{k})$ is a phase factor, which are define by from an A atom and

going out to the three nearest neighbour B atoms:

$$\begin{aligned} t &= \int \phi_\pi^*(\vec{r} - \vec{R}_{u'A}) H \phi_\pi(\vec{r} - \vec{R}_{uB}) d\vec{r}, \\ s &= \int \phi_\pi^*(\vec{r} - \vec{R}_{u'A}) \phi_\pi(\vec{r} - \vec{R}_{uB}) d\vec{r}, \\ f(\vec{k}) &= e^{ik_x a/\sqrt{3}} + 2e^{-ik_x a/2\sqrt{3}} cos(\frac{k_y a}{2}). \end{aligned} \tag{2.25}$$

Then the explicit form of the Hamiltonian and overlap matrix can be written as,

$$H = \begin{pmatrix} \epsilon_{2\mathrm{p}} & tf(\vec{k}) \\ tf^*(\vec{k}) & \epsilon_{2\mathrm{p}} \end{pmatrix}, \tag{2.26}$$

and

$$S = \begin{pmatrix} 1 & sf(\vec{k}) \\ sf^*(\vec{k}) & 1 \end{pmatrix}. \tag{2.27}$$

Solving the secular equation Eq. (2.15) yields the energy eigenvalues:

$$E^v(\vec{k}) = \frac{\epsilon_{2\mathrm{p}} + tw(\vec{k})}{1 + sw(\vec{k})}, \tag{2.28}$$

$$E^c(\vec{k}) = \frac{\epsilon_{2\mathrm{p}} - tw(\vec{k})}{1 + sw(\vec{k})}, \tag{2.29}$$

where the band index b = v, c indicates the valence and conduction bands, $t < 0$, and $w(\vec{k})$ is the absolute value of the phase factor $f(\vec{k})$, i.e $w(\vec{k}) = \sqrt{f^*(\vec{k}) f(\vec{k})}$,

$$w(\vec{k}) = \sqrt{|\ f(\vec{k})\ |^2} = \sqrt{1 + 4\cos\frac{\sqrt{3}k_x a}{2}\cos\frac{k_y a}{2} + 4\cos^2\frac{k_y a}{2}}. \tag{2.30}$$

According to Eq. (2.29), the atomic orbital energy ϵ_{2p} is an arbitrary reference point in the orthogonal STB model ($s = 0$). Substituting the energy eigen value $E^b(\vec{k})$ to

Eq. (2.2)

$$\{\epsilon_{2\mathrm{p}} - E^b(\vec{k})\}C_A^b(\vec{k}) + f(\vec{k})\{t - sE^b(\vec{k})\}C_B^b(\vec{k}) = 0,$$
$$f^*(\vec{k})\{t - sE^b(\vec{k})\}C_A^b(\vec{k}) + \{\epsilon_{2\mathrm{p}} - E^b(\vec{k})\}C_B^b(\vec{k}) = 0, \tag{2.31}$$

we get,

$$C_A^v(\vec{k}) = \frac{f(\vec{k})}{w(\vec{k})}C_B^v(\vec{k}), \quad C_B^v(\vec{k}) = \frac{f^*(\vec{k})}{w(\vec{k})}C_A^v(\vec{k}), \quad \text{for} \quad b = v,$$
$$C_A^c(\vec{k}) = \frac{f(\vec{k})}{w(\vec{k})}C_A^c(\vec{k}), \quad C_B^c(\vec{k}) = \frac{f^*(\vec{k})}{w(\vec{k})}C_A^c(\vec{k}), \quad \text{for} \quad b = c. \tag{2.32}$$

The orthonormal condition for the electron wave function of Eq. (2.6) can be expressed interms of the Bloch wave functions,

$$\begin{aligned}\langle \Psi^{b'}(\vec{k},\vec{r}) \mid \Psi^b(\vec{k},\vec{r})\rangle =& \sum_{s'}^{A,B}\sum_{s}^{A,B} C_{s'}^{b'*}(\vec{k})C_s^b(\vec{k})S_{s's}(\vec{k}) \\ =& C_A^{b'*}(\vec{k})C_A^b(\vec{k}) + sf(\vec{k})C_A^{b'*}(\vec{k})C_B^b(\vec{k}) \\ & + sf^*(\vec{k})C_B^{b'*}(\vec{k})C_A^b(\vec{k}) + C_B^{b'*}(\vec{k})C_B^b(\vec{k}) \\ =& \delta_{b'b}, \quad (b', b = v, c).\end{aligned} \tag{2.33}$$

Thus, we obtain the wave function coefficient $C_A^b(\vec{k})$ and $C_B^b(\vec{k})$ for π electrons which are related to each other by complex conjugation for valence band b=v,

$$C_A^v(\vec{k}) = \sqrt{\frac{f(\vec{k})}{2w(\vec{k})\{1 + sw(\vec{k})\}}}, \quad C_B^v(\vec{k}) = \sqrt{\frac{f^*(\vec{k})}{2w(\vec{k})\{1 + sw(\vec{k})\}}}, \tag{2.34}$$

and for valence band b=c,

$$C_A^c(\vec{k}) = \sqrt{\frac{f(\vec{k})}{2w(\vec{k})\{1 - sw(\vec{k})\}}}, \quad C_B^c(\vec{k}) = -\sqrt{\frac{f^*(\vec{k})}{2w(\vec{k})\{1 - sw(\vec{k})\}}}. \tag{2.35}$$

Fitting the dispersion relations of the graphene sheet given by Eq. (2.29) to the

Fig. 2-3: figure/pi1.pdf

energy values obtained from an *ab initio* calculation gives the values of the transfer integral $t = -3.033$eV and overlap integral $s = 0.129$, and set the atomic orbital energy equal to zero of the energy scale, $\epsilon_{2p} = 0\,\mathrm{eV}$ [1]. Fig. 2-3(a) shows the dispersion relations of the graphene sheet given by Eq. (2.29) with the above parameters throughout the entire area of the first Brillouin zone. The lower (valence) band is completely filled with electrons in the ground state, while the upper (conduction) band is completely empty of electrons in the ground state. The band structure of a graphene sheet shows linear dispersion relations around the K and K′ points near the Fermi level, as can be seen in Fig 2-3(b). The electron wavevector around the K point in the first Brillouin zone can be written in the form $k_x = \Delta k_x$ and $k_y = -4\pi/(3a) + \Delta k_y$, where Δk_x and Δk_y are small compared to $1/a$. Substituting this wavevector into

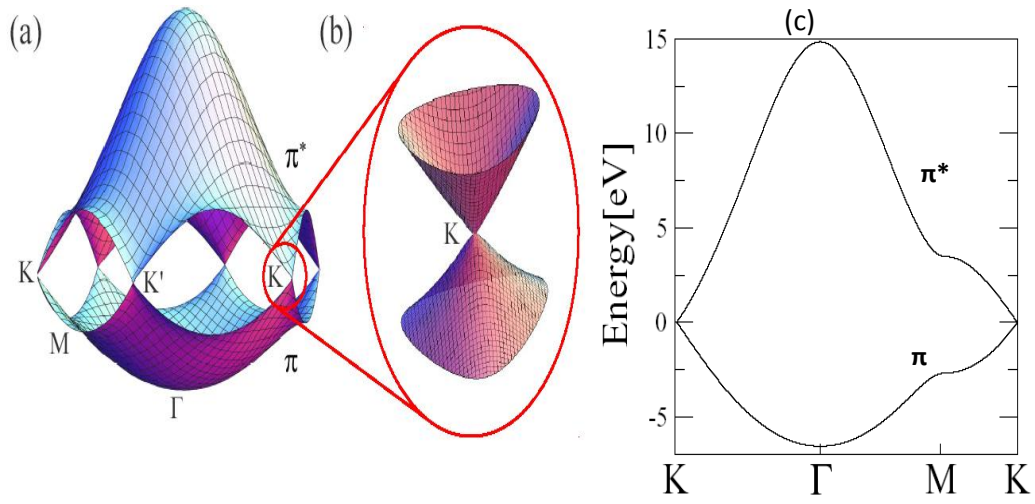

Figure 2-3: The π bands of graphene within the simple tight-binding method. In (a), the energy dispersion is shown throughout the whole region of the Brillouin zone. (b) Near the K point, the energy dispersion relation is approximately linear, showing two symmetric cone shapes, the so-called Dirac cones. (c)The energy dispersion along the high symmetry pionts K, Γ,M and K The tight binding parameters used here are $\epsilon_{2p} = 0\,\mathrm{eV}$, $t = -3.033\,\mathrm{eV}$, and $s = 0.129$.

Eq. (2.29) and making the expansion in a power series in $\Delta k_x a$ and $\Delta k_y a$ up to the second order, $w = \frac{\sqrt{3}}{2}\Delta k a$ can be obtained, where $\Delta k = \sqrt{\Delta k_x^2 + \Delta k_y^2}$ is the distance from the electron wavevector to the K point. Substituting w into Eq. (2.29) gives the electronic dispersion relations in the valence and conduction bands:

$$E^v(\Delta k) = \varepsilon_{2p} - \frac{\sqrt{3}}{2}(\varepsilon_{2p}s - t)\, a\, \Delta k\,, \quad E^c(\Delta k) = \varepsilon_{2p} + \frac{\sqrt{3}}{2}(\varepsilon_{2p}s - t)\, a\, \Delta k\,, \quad (2.36)$$

which are linear in Δk. The linear dispersion relations near the Fermi level suggest that the effective mass approximation of the non-relativistic Schrödinger equation used for conventional semiconductors with parabolic energy bands is not applicable to a graphene sheet. The conducting π electrons in a graphene sheet mimic massless particles whose behavior is described by the relativistic Dirac equation. Furthermore, the linear dispersion relations increase the mobility of the conducting π electrons in a graphene sheet compared to conventional semiconductors. The energy surface changes from circle to triangle with increasing distance from the K point, giving rise to the so-called trigonal warping effect [25].

2.2.2 σ band of two dimensional graphene

In 2D graphene, three orbitals 2s, $2p_x$ and $2p_y$ mixed to one another and form covalent σ bonds, which are responsible for the graphene hexagonal lattice structure. Graphene unit cell has two carbon atoms has six orbitals give six σ energy bands. To calculate this sigma bands, 6×6 Hamiltonian and overlap matrix need to be constructed. After that the secular equation should be solved for each $\vec{k}$ points. The 6×6 Hamiltoinian and the overlap matrices are composed of two 3×3 submatrix. We can identify the atomic orbital according to their position in two carbon atom A and B in graphene unit cell. These are $2s_A$, $2p_x^A$, $2p_y^A$, $2s^B$, $2p_x^B$, and $2p_y^B$. The 3×3 Hamiltonian

submatrix H_{AA} coupling same atoms is a diagonal matrix can be expressed as,

$$
\begin{aligned}
H_{AA}(\vec{k}) &= \begin{pmatrix} \langle 2\mathrm{s}^{\mathrm{A}} \mid H \mid 2\mathrm{s}^{\mathrm{A}} \rangle & \langle 2\mathrm{s}^{\mathrm{A}} \mid H \mid 2\mathrm{p}_{\mathrm{x}}^{\mathrm{A}} \rangle & \langle 2\mathrm{s}^{\mathrm{A}} \mid H \mid 2\mathrm{p}_{\mathrm{y}}^{\mathrm{A}} \rangle \\ \langle 2\mathrm{p}_{\mathrm{x}}^{\mathrm{A}} \mid H \mid 2\mathrm{s}^{\mathrm{A}} \rangle & \langle 2\mathrm{p}_{\mathrm{x}}^{\mathrm{A}} \mid H \mid 2\mathrm{p}_{\mathrm{x}}^{\mathrm{A}} \rangle & \langle 2\mathrm{p}_{\mathrm{x}}^{\mathrm{A}} \mid H \mid 2\mathrm{p}_{\mathrm{y}}^{\mathrm{A}} \rangle \\ \langle 2\mathrm{p}_{\mathrm{y}}^{\mathrm{A}} \mid H \mid 2\mathrm{s}^{\mathrm{A}} \rangle & \langle 2\mathrm{p}_{\mathrm{y}}^{\mathrm{A}} \mid H \mid 2\mathrm{p}_{\mathrm{x}}^{\mathrm{A}} \rangle & \langle 2\mathrm{p}_{\mathrm{y}}^{\mathrm{A}} \mid H \mid 2p_y^A \rangle \end{pmatrix} \\
&= \begin{pmatrix} \langle 2\mathrm{s}^{\mathrm{A}} \mid H \mid 2\mathrm{s}^{\mathrm{A}} \rangle & 0 & 0 \\ 0 & \langle 2\mathrm{p}_{\mathrm{x}}^{\mathrm{A}} \mid H \mid 2\mathrm{p}_{\mathrm{x}}^{\mathrm{A}} \rangle & 0 \\ 0 & 0 & \langle 2\mathrm{p}_{\mathrm{y}}^{\mathrm{A}} \mid H \mid 2\mathrm{p}_{\mathrm{y}}^{\mathrm{A}} \rangle \end{pmatrix} \\
&= \begin{pmatrix} \epsilon_{2\mathrm{s}} & 0 & 0 \\ 0 & \epsilon_{2\mathrm{p}} & 0 \\ 0 & 0 & \epsilon_{2\mathrm{p}} \end{pmatrix} \\
&= H_{BB}(\vec{k}),
\end{aligned} \tag{2.37}
$$

where $\epsilon_{2\mathrm{p}}$ is the orbital energy of the 2p levels and $\epsilon_{2\mathrm{s}}$ is the orbital energy of 2s levels. The 3×3 Hamiltonian submatrix H_{AB} considering the nearesr neighbor atoms is,

$$
H_{AB}(\vec{k}) = \begin{pmatrix} \langle 2\mathrm{s}^{\mathrm{A}} \mid H \mid 2\mathrm{s}^{\mathrm{B}} \rangle & \langle 2\mathrm{s}^{\mathrm{A}} \mid H \mid 2\mathrm{p}_{\mathrm{x}}^{\mathrm{B}} \rangle & \langle 2\mathrm{s}^{\mathrm{A}} \mid H \mid 2\mathrm{p}_{\mathrm{y}}^{\mathrm{B}} \rangle \\ \langle 2\mathrm{p}_{\mathrm{x}}^{\mathrm{A}} \mid H \mid 2\mathrm{s}^{\mathrm{B}} \rangle & \langle 2\mathrm{p}_{\mathrm{x}}^{\mathrm{A}} \mid H \mid 2\mathrm{p}_{\mathrm{x}}^{\mathrm{B}} \rangle & \langle 2\mathrm{p}_{\mathrm{x}}^{\mathrm{A}} \mid H \mid 2\mathrm{p}_{\mathrm{y}}^{\mathrm{B}} \rangle \\ \langle 2\mathrm{p}_{\mathrm{y}}^{\mathrm{A}} \mid H \mid 2\mathrm{s}^{\mathrm{A}} \rangle & \langle 2\mathrm{p}_{\mathrm{y}}^{\mathrm{A}} \mid H \mid 2\mathrm{p}_{\mathrm{x}}^{\mathrm{A}} \rangle & \langle 2\mathrm{p}_{\mathrm{y}}^{\mathrm{A}} \mid \mathrm{H} \mid 2\mathrm{p}_{\mathrm{y}}^{\mathrm{B}} \rangle \end{pmatrix} \tag{2.38}
$$

We can resolve the Bloch orbitals $2\mathrm{p}_{\mathrm{x}}$ and $2\mathrm{p}_{\mathrm{y}}$ in A and B atomic positions in the direction parallel and perpendicular to the bond direction. After that we can calculate the matrix elements of Eq. (2.38). Let us take an example of $\langle 2\mathrm{p}_{\mathrm{x}}^{\mathrm{A}} \mid H \mid 2\mathrm{p}_{\mathrm{y}}^{\mathrm{B}} \rangle$. In Fig. 2-4 shows how to calculate the Hamiltonian matrix element. In the Fig. 2-4 there are three nearest A atoms for the B atom in center. Three A atom has $2\mathrm{p}_{\mathrm{x}}$ orbital and center B atom has one $2\mathrm{p}_{\mathrm{y}}$ orbital.

Fig. 2-4: fig/sig32.pdf

We can write the phase factor for three nearest neighbor as

$$\begin{aligned} p1 &= \exp[i\vec{k}\cdot\vec{r}^{1}_{A}] \\ p2 &= \exp[i\vec{k}\cdot\vec{r}^{2}_{A}] \\ p3 &= \exp[i\vec{k}\cdot\vec{r}^{3}_{A}] \end{aligned} \tag{2.39}$$

After taking parallel and perpendicular component of $2p_x$ and $2p_y$ orbital along the bond direction, we got integrals which is know as π and σ transfer and overlap integrals. $\frac{\sqrt{3}}{4}$ appear from the parallel and perpendicular component of $2p_y^B$ at center

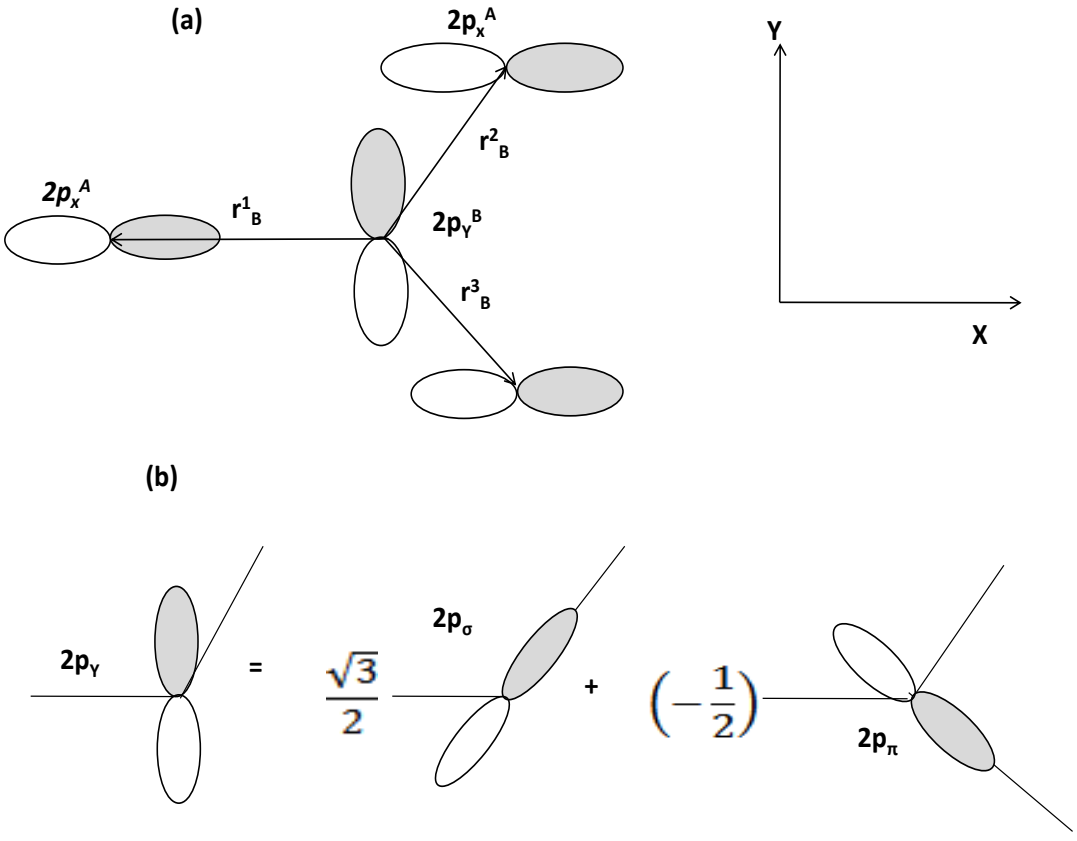

Figure 2-4: (a)Three $2p_x$ orbitals at three A atoms and one $2p_y$ orbitals at central B atom. (b)The rotation of $2p_y$. The component along the bond direction is $2p_\sigma$, component perpendicular to the bond direction is $2p_\pi$.

B atom and $2p_x^A$ at R_A^3. The other matrix elements can be can be calculated by the same way and are given by

$$\langle 2s^A \mid H \mid 2s^B \rangle = H_{ss}(p1 + p2 + p3) \tag{2.40}$$

$$\langle 2p_x^A \mid H \mid 2s^B \rangle = H_{ss}(p1 - \frac{p2}{2} - \frac{p3}{2}) \tag{2.41}$$

$$\langle 2p_y^A \mid H \mid 2p_y^B \rangle = \frac{\sqrt{3}}{2} H_{sp}(-p2 + p3) \tag{2.42}$$

$$\langle 2s^A \mid H \mid 2p_x^B \rangle = \frac{\sqrt{3}}{2} H_{sp}(-p1 + \frac{p2}{2} + \frac{p3}{2}) \tag{2.43}$$

$$\langle 2p_x^A \mid H \mid 2p_x^B \rangle = H_{\sigma}(\frac{-p1 - p2 - p3}{4}) + \frac{3}{4} H_{\pi}(p2 + p3) \tag{2.44}$$

$$\langle 2p_y^A \mid H \mid 2p_x^B \rangle = \frac{\sqrt{3}}{4}(H_{\sigma} + H_{\pi})(p2 - p3) \tag{2.45}$$

$$\langle 2s^A \mid H \mid 2p_y^B \rangle = \frac{\sqrt{3}}{2} H_{sp}(p2 - p3) \tag{2.46}$$

$$\langle 2p_x^A \mid H \mid 2p_y^B \rangle = \frac{\sqrt{3}}{4}(H_{\sigma} + H_{\pi})(p2 - p3) \tag{2.47}$$

$$\langle 2p_y^A \mid H \mid 2p_y^B \rangle = -\frac{3}{4} H_{\sigma}(p2 + p3) + H_{\pi}(p1 + \frac{p2 + p3}{4}) \tag{2.48}$$

$$\langle 2p_y^A \mid H \mid 2p_y^B \rangle = H_{\pi}(p1 + p2 + p3) \tag{2.49}$$

The table 2.1[1] below show the list of tight binding parameters which is used to calculate the matrix element given in Eq.(2.40-2.49)

Table 2.1: Tight binding parameters for graphene

H	value(eV)	S	value
H_{ss}	-6.769	S_{2s2s}	0.212
H_{sp}	-5.580	S_{2s2p}	0.102
H_{σ}	-5.037	S_{2s2p}	0.146
H_{π}	-3.033	S_{π}	0.129
ϵ_{2s}	-8.868		

Here the H denote the tight binding parameter for Hamiltonian matrix elements in eV and S denote the overlap integral.

Fig. 2-5: fig/allbnd1.pdf

2.3 X-ray absorption in graphene

In this section, we nowdescribe how to calculate the electron-photon matrix element when X-ray excite the core electons to the π^* and σ^* bands. We will use first order perturbation theory and tight binding electron wave function for 1s core electron, $2p_z$ orbital for π electron, and σ electrons which is a mixed states of 2s, $2p_x$ and $2p_y$ orbtals. These σ electrons wave functions in the solid can be expressed as the linear combination of Bloch functions for 2s, $2p_x$ and $2p_y$ orbitals.

2.3.1 Dipole approximation

When an electromagnetic wave having an electromagnetic field with vector potential $\vec{A}$ interact with a charge particle in a solid crystal with periodic crystal potential V(r)

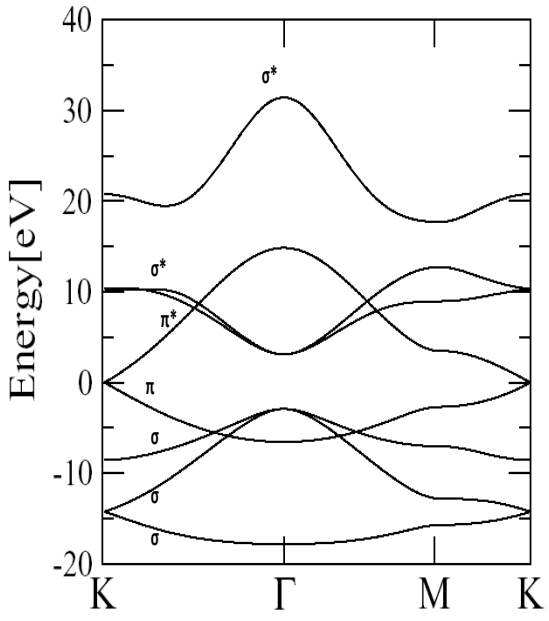

Figure 2-5: The energy dispersion relations of π and σ band of 2D graphene along the high symmetry points K, Γ,M and K

of mass m, charge e of the electron in the Hamiltonian can be expressed as

$$H = \frac{1}{2m}\{-i\hbar\nabla - e\vec{A}(t)\}^2 + V(\vec{r}). \tag{2.50}$$

The wave functions for initial and final states are the eigen states of an unperturbed Hamiltonian $H_o = -\frac{\hbar^2}{2m}\Delta + V(\vec{r})$. When we neglect the quadratic terms in $\vec{A}(t)$ and uses the coulomb gauge $\nabla \cdot \vec{A}(t) = 0$, the perturbation Hamiltonian $H_{\text{opt},\rho}$ acting on the electron and causing it transition from core electronic state to the unoccupied states is given by,

$$H_{\text{opt},\rho} = \frac{ie\hbar}{m}\vec{A}(t) \cdot \nabla \tag{2.51}$$

Where $\rho = A, E$ stands for absorption and emission of light respectively. The Maxwell equation which we need is in SI unit given by,

$$\nabla \times \vec{B} = \epsilon_0\mu_0\frac{\delta\vec{E}}{\delta t}. \tag{2.52}$$

The electric and the magnetic field of the light are $\vec{E}_\rho(t) = \vec{E}_0 \exp[i(\vec{k} \cdot \vec{r} \pm \omega t)]$ and $\vec{B}_\rho(t) = \vec{E}_0 \exp[i(\vec{k}.\vec{r} \pm \omega t)]$ respectively. Thus, $\vec{B} = \nabla \times \vec{A} = i\vec{k} \times \vec{A}$ and $\nabla \times \vec{B} = ik \times \vec{B}$. We can write, $\nabla \times \vec{B} = k^2\vec{A} = \frac{1}{c^2}\frac{\delta\vec{E}}{\delta t}$. Since E is a plane wave we just get $\frac{\delta\vec{E}}{\delta t} = -i\omega\vec{E}$ then using $\omega = kc$ we can write $\vec{A}$ in vacuum as, $A_\rho = -\frac{i\vec{E}}{\omega}$. The energy densiy I_ρ of the electromagnetic wave is given by,

$$I_\rho = \frac{E_\rho B_\rho}{\mu_o} = \frac{E_\rho^2}{\mu_o c}. \tag{2.53}$$

The unit of I_ρ is [J/m^{2}sec]. The vector potential can be written in terms of the of the light intensity I_ρ, and the polarization of the electric field component $\vec{P}$ as,

$$A_\rho(t) = \frac{-i}{w}\sqrt{\frac{I_\rho}{c\epsilon_o}}\exp(\pm i\omega t)\vec{P}. \tag{2.54}$$

The Matrix element for the optical transitions from an initial state i at $\vec{k}$=$\vec{k_i}$ to a final state f at $\vec{k}$=$\vec{k_f}$ is defined by,

$$M^{fi}_{\rm opt}(\vec{k}_f, \vec{k}_i) = \langle \Psi^f(\vec{k}_f) \mid H_{{\rm opt},\rho} \mid \Psi(\vec{k}_i) \rangle. \tag{2.55}$$

the matrix element in Eq. (2.55) is calculated by,

$$M^{fi}_{\rm opt}(\vec{k}_f, \vec{k}_i) = \frac{e\hbar}{m\omega_\rho}\sqrt{\frac{I_\rho}{c\epsilon_o}}\exp[i(\omega_f - w_i \pm \omega_\rho)t]\vec{D}(\vec{k}_f, \vec{k}_i)\cdot\vec{P} \tag{2.56}$$

where

$$\vec{D}(\vec{k}_f, \vec{k}_i) = \langle \Psi^f(\vec{k}_f) \mid \nabla \mid \Psi(\vec{k}_i) \rangle. \tag{2.57}$$

Ψ^i and Ψ^f are the tight binding wave function for the inital and the final state. The Fermi golden rule gives the transition probabilities perunit time from initial states i to final state f. The transition probability per one second as a function $\vec{k}$ can be expressed as,

$$W(\vec{k}_f, \vec{k}_i) = \frac{4e^2\hbar^4 I_\rho}{\tau\epsilon_o m^2 c^3 E^2_{\rm x}} \mid \vec{P}\cdot\vec{D}^{fi}(\vec{k}_f, \vec{k}_i) \mid^2 \frac{\sin^2[(E^f(\vec{k}_f) - E^i(\vec{k}_i) \pm E_{\rm x})\frac{\tau}{2\hbar}}{(E^f(\vec{k}_f) - E^i(\vec{k}_i) \pm E_{\rm x})^2}. \tag{2.58}$$

Where ϵ_o is the dielectric constant of the vacuum. In case of the real sample, we need to replace ϵ_o by $\epsilon\epsilon_o$. ϵ in the effective dielectric constant of the sample. If the interaction time τ is long then the energy conservation $E^f(\vec{k}_f) - E^i(\vec{k}_i) = 0$ is fulfilled, since $\dfrac{\sin^2(\alpha t)}{\pi\alpha^2 t} \rightarrow \delta(\alpha)$ for $\tau \rightarrow \infty$. The Absorption intensity $I(E)$ as a function of energy E can be calculated by integrating the $W(k)$ along the equienergy contour line and can be expressed as,

$$I(E) = \int_E W(\vec{k}_f, \vec{k}_i)dk \tag{2.59}$$

$$= \frac{4e^2\hbar^4 I_\rho}{\tau\epsilon_o m^2 c^3 E^2_x}\int_E \mid \vec{P}.\vec{D}^{fi}(\vec{k}_f, \vec{k}_i) \mid^2 \rho(E)dk \tag{2.60}$$

where $\rho(E)$ is the density of states at energy E. The above equation is important because now the X-ray absorption intensity depends on two imporant parts; one is the

matrix element $\mid \vec{P} \cdot \vec{D}^{fi}(\vec{k}_f, \vec{k}_i) \mid^2$ which is the square of the inner product of dipole vector and and polarization vector and the other part is $\rho(E)$, the density of states (DOS) which is a function of X-ray energy. Thus, as the angle between the dipole vector $\vec{D}(\vec{k})$ and polarization vector $\vec{P}$ changes the absorption intensity changes. In the next section, we will derive an equation for the dipole vector for 1s to π^* and 1s to σ^* transtion.

2.3.2 Dipole vector

In the X-ray absorption spectra, the inital state is 1s core electronic orbital and the final state is the unoccupied π^* state and the σ^* state. Let us write down the initial state and the final state in terms of the Bloch function Φ_A and Φ_B at atomic site A and B. This Bloch function can decompose into the atomic orbitals with the Bloch phase factors. In the X-ray absorption process optical transition within the same atom and between the atoms are possible. Transition within the same atom is defined as on-site interaction and transition between the neighboring atoms is defined as off-site interaction.

In case of 1s to π^* transition, the X-ray absorption for both on-site and off-site interaction is possible because of the even symmetry of the dipole vector in z diraction. Generally, in the core excitation process like X-ray absorption, the on-site interaction dominated in the total absorption process beacuse of the strong overlaping of localized wave function of core elctrons and final state wave functions. Such overlapping is weak in the off-site interaction.

$$\Psi^{1s}(\vec{k}) = C_A^{1s}(\vec{k})\Phi_A(\vec{k}, \vec{r}) + C_B^{1s}(\vec{k})\Phi_B(\vec{k}, \vec{r}). \tag{2.61}$$

$$\Psi^{2p_z}(\vec{k}) = C_A^{2p_z}(\vec{k})\Phi_A(\vec{k}, \vec{r}) + C_B^{2p_z}(\vec{k})\Phi_B(\vec{k}, \vec{r}). \tag{2.62}$$

Fig. 2-6: figure/neibor_d.pdf

$$\begin{aligned}\Psi^{\sigma}(\vec{k}) =& C_A^{2s}(\vec{k})\Phi_A(\vec{k},\vec{r}) + C_A^{2p_x}(\vec{k})\Phi_A(\vec{k},\vec{r}) \\ &+ C_A^{2p_y}(\vec{k})\Phi_A(\vec{k},\vec{r}) + C_B^{2s}(\vec{k})\Phi_B(\vec{k},\vec{r}) \\ &+ C_B^{2p_x}(\vec{k})\Phi_B(\vec{k},\vec{r}) + C_A^{2p_y}(\vec{k})\Phi_A(\vec{k},\vec{r}). \end{aligned} \tag{2.63}$$

The dipole vector for $1s$ to π^* transition can be expressed as,

$$\begin{aligned}\vec{D}(\vec{k_f},\vec{k_i}) =& C_A^{f^*}(\vec{k_f})C_A^{i}(\vec{k_i})\langle\Phi_A(\vec{k_f},\vec{r}) \mid \nabla \mid \Phi_A(\vec{k_i},\vec{r})\rangle \\ &+ C_B^{f^*}(\vec{k_f})C_B^{i}(\vec{k_i})\langle\Phi_B(\vec{k_f},\vec{r}) \mid \nabla \mid \Phi_B(\vec{k_i},\vec{r})\rangle \\ &+ C_A^{f^*}(\vec{k_f})C_B^{i}(\vec{k_i})\langle\Phi_A(\vec{k_f},\vec{r}) \mid \nabla \mid \Phi_B(\vec{k_i},\vec{r})\rangle \\ &+ C_B^{f^*}(\vec{k_f})C_A^{i}(\vec{k_i})\langle\Phi_B(\vec{k_f},\vec{r}) \mid \nabla \mid \Phi_A(\vec{k_i},\vec{r})\rangle. \end{aligned} \tag{2.64}$$

where i is the initaial state 1s orbital and f is final state π^* orbital. We will now substitute Bloch functions to the tight binding atomic wave functions. The coordinates of all the atoms in the crystal can be split in to $\vec{R}_A^j$ and $\vec{R}_B^j$ over the A and B sublatticeS. If the transtion is from A to B atom we use vectors $\vec{r}_A^{\,l}$ and if the off site transtion is from B to atom then we use the vector $\vec{r}_b^{\,l}$. The vector $\vec{r}_A^{\,l}(\vec{r}_B^{\,l})$ connect $A(B)$ atom to the nearest neighbor atom shown in Fig 2-6.

$$\vec{R}_A^j = \vec{R}_B^i + \vec{r}_B^{\,l}, \quad \vec{R}_B^j = \vec{R}_A^i + \vec{r}_A^{\,l}, \quad (l = 1,2,3) \tag{2.65}$$

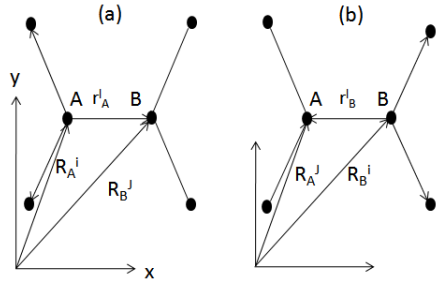

Figure 2-6: Position vectors and the conecting vectors between the nearest neighbor when (a) the center atom is A and (b) the center atom is B.

$$\vec{D}(\vec{k_f},\vec{k_i}) = \vec{D}^{\rm on}(\vec{k_f},\vec{k_i}) + \vec{D}^{\rm off}(\vec{k_f},\vec{k_i}). \tag{2.66}$$

$$\begin{aligned}
\vec{D}^{\rm on}(\vec{k_f},\vec{k_i}) =& C_A^{f^*}(\vec{k_f})C_A^i(\vec{k_i})\langle\Phi_A(\vec{k_f},\vec{r}) \mid \nabla \mid \Phi_A(\vec{k_i},\vec{r})\rangle \\
&+ C_B^{f^*}(\vec{k_f})C_B^i(\vec{k_i})\langle\Phi_B(\vec{k_f},\vec{r}) \mid \nabla \mid \Phi_B(\vec{k_i},\vec{r})\rangle, \\
=& C_A^{f^*}(\vec{k_f})C_A^i(\vec{k_i})\langle\phi_f(\vec{r}) \mid \nabla \mid \phi_i(\vec{r})\rangle + C_B^{f^*}(\vec{k_f})C_B^i(\vec{k_i})\langle\phi_f(\vec{r}) \mid \nabla \mid \phi_i(\vec{r})\rangle, \\
=& C_A^{f^*}(\vec{k_f})C_A^i(\vec{k_i})m_{\rm opt}^{AA}\hat{\vec{z}} + C_B^{f^*}(\vec{k_f})C_B^i(\vec{k_i})m_{\rm opt}^{BB}\hat{\vec{z}}.
\end{aligned} \tag{2.67}$$

No Bloch phase factor appear in the above equation because X-ray absortion is within the same atom. Where $m_{\rm opt}^{AA} = m_{\rm opt}^{AA} = \langle\phi_f(\vec{r}) \mid \nabla \mid \phi_i(r)\rangle$ is an atomic matrix element for on-site interaction and it directed along the perpendicular direction of graphene plane (z) in case of 1s to π^* transition. $\phi_i(r)$ and $\phi_f(r)$ is the atomic orbital wave function of initial and final states. Now let us derive the expression for 1s to π^* off-site transtion.

$$\begin{aligned}
\vec{D}^{\rm off}(\vec{k_f},\vec{k_i}) =& C_A^{f^*}(\vec{k_f})C_B^i(\vec{k_i})\langle\Phi_A(\vec{k_f},\vec{r}) \mid \nabla \mid \Phi_B(\vec{k_i},\vec{r})\rangle \\
&+ C_B^{f^*}(\vec{k_f})C_A^i(\vec{k_i})\langle\Phi_B(\vec{k_f},\vec{r}) \mid \nabla \mid \Phi_A(\vec{k_i},\vec{r})\rangle, \\
=& \frac{1}{U}\sum_{i=0}^{U-1}\sum_{l=1}^{3} C_B^{f^*}(\vec{k_f})C_A^i(\vec{k_i})\exp[i(\vec{k_i}-\vec{k_f})\cdot\vec{R}_A^i] \\
&\times \exp[-i\vec{k_f}\cdot\vec{r}_A^{\,l}]\langle\phi_f(\vec{r}-\vec{r}_A^{\,l}) \mid \nabla \mid \phi_i(\vec{r})\rangle \\
&+ \frac{1}{U}\sum_{i=0}^{U-1}\sum_{l=1}^{3} C_A^{f^*}(\vec{k_f})C_B^i(\vec{k_i})\exp[i(\vec{k_i}-\vec{k_f})\cdot\vec{R}_B^i] \\
&\times \exp(-i\vec{k_f}\cdot\vec{r}_B^{\,l})\langle\phi_f(\vec{r}-\vec{r}_B^{\,l}) \mid \nabla \mid \phi_i(\vec{r})\rangle, \\
=& C_B^{f^*}(\vec{k_f})C_A^i(\vec{k_i})\sum_{l=1}^{3}\exp(-i\vec{r}_A^{\,l}\cdot\vec{k})\int \phi_f(\vec{r}-\vec{r}_A^{\,l})\nabla\phi_i(\vec{r})\hat{\vec{z}} \\
&+ C_A^{f^*}(\vec{k_f})C_B^i(\vec{k_i})\sum_{l=1}^{3}\exp(-i\vec{r}_A^{\,l}\cdot\vec{k})\int \phi_f(\vec{r}-\vec{r}_B^{\,l})\nabla\phi_i(\vec{r})\hat{\vec{z}}.
\end{aligned} \tag{2.68}$$

In case of 1s to π^* off site transition, where the intial states is in 1s state orbital and

final state is in the π^* states, the dipole vector can be written as,

$$\begin{aligned}\vec{D}^{\text{off}}(\vec{k_f},\vec{k_i}) =& C_B^{f^*}(\vec{k_f})C_A^i(\vec{k_i})\sum_{l=1}^{3}\exp(-i\vec{r}_A^{\,l}\cdot\vec{k_f})m_{\text{opt}}^{AB}\hat{\vec{z}} \\ &+ C_A^{f^*}(\vec{k_f})C_B^i(\vec{k_i})\sum_{l=1}^{3}\exp(-(i\vec{r}_B^{\,l}\cdot\vec{k_f})m_{\text{opt}}^{BA}\hat{\vec{z}}. \end{aligned} \tag{2.69}$$

$\hat{\vec{z}}$ is the unit vector along z direction.

For 1s to σ^* transntion, the X-ray absorption for both on-site and off-site interaction is possible because of the even symmetry of the dipole vector in x and y direction We can expressed the dipole vector for 1s to σ^* transition interms of off-site and on-site interaction.

$$\vec{D}(\vec{k_f},\vec{k_i}) = \vec{D}^{\text{on}}(\vec{k_f},\vec{k_i}) + \vec{D}^{\text{off}}(\vec{k_f},\vec{k_i}), \tag{2.70}$$

The wave function of electron the final state σ^* can be expressed as summation of the Bloch functions for 2s,2p_x and 2p_y at the atomic position A and B.

$$\Psi(\vec{k}_i,\vec{k}_f) = \sum_{s=2\text{s}^\text{A}\ldots2\text{p}_\text{y}^\text{B}} C_s^j(\vec{k})\Phi_s(\vec{k},\vec{r}). \tag{2.71}$$

Thus the dipole vector can be written as,

$$\vec{D}(\vec{k_f},\vec{k_i}) = \sum_{i,j=A,B}\ \sum_{o=2\text{s},2\text{p}_\text{x},2\text{p}_\text{y};\text{o}'=1\text{s}} C_i^{o^*}(\vec{k_f})C_j^{o'}(\vec{k_i})\langle\Phi_i^o(\vec{k}_f,\vec{r}) \mid \nabla \mid \Phi_j^{o'}(\vec{k}_i,\vec{r})\rangle. \tag{2.72}$$

We can isolate the on-site and off-site dipole vector part as follows,

$$\begin{aligned}\vec{D}^{\text{on}}(\vec{k_f},\vec{k_i}) &= \sum_{i=j=A,B}\ \sum_{o=2\text{s},2\text{p}_\text{x},2\text{p}_\text{y};\text{o}'=1\text{s}} C_i^{o^*}(\vec{k_f})C_j^{o'}(\vec{k_i})\langle\Phi_i^o(\vec{k}_f,\vec{r}) \mid \nabla \mid \Phi_j^{o'}(\vec{k}_i,\vec{r})\rangle. \\ \vec{D}^{\text{off}}(\vec{k_f},\vec{k_i}) &= \sum_{i\neq j=A,B}\ \sum_{o=2\text{s},2\text{p}_\text{x},2\text{p}_\text{y};\text{o}'=1\text{s}} C_i^{o^*}(\vec{k_f})C_j^{o'}(\vec{k_i})\langle\Phi_i^o(\vec{k}_f),\vec{r}) \mid \nabla \mid \Phi_j^{o'}(\vec{k}_i,\vec{r})\rangle. \end{aligned} \tag{2.73}$$

After expanding the Bloch function interms of the atomic orbital the on-site dipole

vector define in Eq. (2.73) is expressed as,

$$\begin{aligned}
\vec{D}^{\mathrm{on}}(\vec{k_f},\vec{k_i}) =& C_A^{2\mathrm{p}_\mathrm{x}^*}(\vec{k_f})C_A^{1\mathrm{s}}(\vec{k_i})\langle\phi_A^{2\mathrm{p}_\mathrm{x}}(\vec{r}) \mid \nabla \mid \phi_A^{1\mathrm{s}}(\vec{k_i},\vec{r})\rangle \\
&+ C_A^{2\mathrm{p}_\mathrm{y}^*}(\vec{k_f})C_A^{1\mathrm{s}}(\vec{k_i})\langle\phi_A^{2\mathrm{p}_\mathrm{y}}(\vec{r}) \mid \nabla \mid \phi_A^{1\mathrm{s}}(\vec{r})\rangle \\
=& C_A^{2\mathrm{p}_\mathrm{x}^*}(\vec{k_f})C_A^{1\mathrm{s}}(\vec{k_i})\int \phi_A^{2\mathrm{p}_\mathrm{x}}(\vec{r})\nabla\phi_A^{1s}(\vec{k_i},\vec{r})d\vec{r} \\
&+ C_A^{2\mathrm{p}_\mathrm{y}^*}(\vec{k_f})C_A^{1\mathrm{s}}(\vec{k_i})\int \phi_A^{2\mathrm{p}_\mathrm{y}}(\vec{r})\nabla\phi_A^{1s}(\vec{r})\vec{r}d\vec{r} \\
=& C_A^{2\mathrm{p}_\mathrm{x}^*}(\vec{k_f})C_A^{1\mathrm{s}}(\vec{k_i})m_{\mathrm{opt}}^{AA}\hat{\vec{x}} + C_A^{2\mathrm{p}_\mathrm{y}^*}(\vec{k_f})C_A^{1\mathrm{s}}(\vec{k_i})m_{\mathrm{opt}}^{AA}\hat{\vec{y}}.
\end{aligned} \tag{2.74}$$

Where $\hat{\vec{x}}$ and $\hat{\vec{y}}$ are the unit vector along x and y direction. As we know that σ orbital is a mixing of 2s, $2\mathrm{p}_\mathrm{x}$, and $2\mathrm{p}_\mathrm{y}$ orbital, for the simplicity we will only consider A to B off-site transition to calculate off-site dipole vector. The off-site dipole vector for 1s to σ^* can be written as,

$$\vec{D}^{\mathrm{off}}(\vec{k_{\sigma^*}},\vec{k_{1s}}) = \vec{D}^{\mathrm{off}}(\vec{k_{2\mathrm{s}}},\vec{k_{1s}}) + \vec{D}^{\mathrm{off}}(\vec{k_{2\mathrm{p}_\mathrm{x}}},\vec{k_{1s}}) + \vec{D}^{\mathrm{off}}(\vec{k_{2\mathrm{p}_\mathrm{y}}},\vec{k_{1s}}) \tag{2.75}$$

where,

$$\begin{aligned}
\vec{D}^{\mathrm{off}}(\vec{k_{2\mathrm{s}}},\vec{k_{1s}}) =& \frac{2\sqrt{3}m_{\mathrm{off}}^{2\mathrm{s}}}{a}C_B^{2s^*}(\vec{k_{2\mathrm{s}}})C_A^{1\mathrm{s}}(\vec{k_{1\mathrm{s}}})\sum_l \exp\{-(i\vec{r_A^l}.\vec{k})\}\cdot\vec{r_A^l}] \\
\vec{D}^{\mathrm{off}}(\vec{k_{2\mathrm{p}_\mathrm{x}}},\vec{k_{1s}}) =& \frac{2\sqrt{3}m_{\mathrm{off}}^{2\mathrm{p}_\mathrm{x}}}{a}C_B^{2p_x^*}(\vec{k_{2\mathrm{p}_\mathrm{x}}})C_A^{1\mathrm{s}}(\vec{k_{1\mathrm{s}}})\sum_l \exp\{-(i\vec{r_A^l}.\vec{k})\}\cdot\vec{r_A^l}] \\
\vec{D}^{\mathrm{off}}(\vec{k_{2\mathrm{p}_\mathrm{y}}},\vec{k_{1s}}) =& \frac{2\sqrt{3}m_{\mathrm{off}}^{2\mathrm{p}_\mathrm{y}}}{a}C_B^{2p_y^*}(\vec{k_{2\mathrm{p}_\mathrm{y}}})C_A^{1\mathrm{s}}(\vec{k_{1\mathrm{s}}})\sum_l \exp\{-(i\vec{r_A^l}.\vec{k})\}\cdot\vec{r_A^l}]
\end{aligned}$$

We can formulate the oscillation strength $O(\vec{k}_f,\vec{k}_i)$ as the square root of the inner product of the dipole vector.

$$O(\vec{k}_f,\vec{k}_i) = \sqrt{D^{*if}(\vec{k}_f,\vec{k}_i)\cdot D^{if}(\vec{k}_f,\vec{k}_i)}. \tag{2.76}$$

2.3.3 Energy and momentum conservation in X-ray absorption

In the visible range ofthe light, when the photon interacts with the electron in solid, the momentum of electron does not change because of the negligible photon momentum. Thus optical absoprtion occurs at the same k points in the Brillouin zone. Such an inter band transtion is called the vertical transiton. The π-π^* optical absorption in graphene is an example of such vertical transition. The energy and momentum conservation can be expressed as,

$$E_f(k_f) - E_i(k_i) = E_l, k_i + k_l \qquad = k_f, \tag{2.77}$$

$$k_i \approx k_f. \tag{2.78}$$

Here k_i, k_f and k_l are initial momentum of electron in solid, final momentum of electron and k_l is incident light photon momentum. $E_i(k_i)$ and $E_f(k_f)$ are the energy of electron at intial and final state as a function of intitial and final momentum k_i and k_f respectively. E_l is the incident light energy. In case of X-ray absorption in graphene which is core excitation process the minimum photon energy needed to excite the core electron in a carbon atom is around 284eV. Then the final state electron momentum is higher than the intial momentum of electron. Hence, X-ray absorption process is not a vertical transition, instead many final states appear for each intial state. The energy and momentum conservation can be expressed as,

$$\begin{aligned} E_f(k_f) - E_i(k_i) = E_\mathrm{x}, \quad k_i + k_\mathrm{x} \qquad &= k_f, \\ E_\mathrm{x} &= \hbar\omega, \\ &= \hbar c k_\mathrm{x}. \end{aligned} \tag{2.79}$$

Where E_x is the incident X-ray energy energy, k_x is the X-ray photon momentum. c is the speed of light in vacuum, $\hbar$ is the Plank's constant.

2.3.4 Density of states

The densty of states (DOS) in the unit of states/eV/1C-atom can be expresses in terms of summation of the delta function.

$$n(E) = \frac{\int 2 \sum_{\mu=-\frac{N}{2}}^{\frac{N}{2}-1} \sum_{i=-\frac{U}{2}}^{\frac{U}{2}-1} \delta[E - E_\mu(k_i)]dk_i}{\int \sum_{\mu=-\frac{N}{2}}^{\frac{N}{2}-1} \sum_{i=-\frac{U}{2}}^{\frac{U}{2}-1} \delta[E' - E_\mu(k_i)]dk'}. \tag{2.80}$$

the summation is taken over all the U number of unit cells in graphene and the integration taken over for k_i in the Brillouin zone. all the valence and conduction band index by μ. The number 2 comes from spin degeneracy. The δ function can be simulated by Gaussian line shape

$$\delta(E - E_\mu(k_i)) = \exp\left[\frac{-(E - E_\mu(k_i))^2}{2(\Delta E)^2}\right].$$

Joint Density of states (JDOS) is related to experiments that measure the absorption of light and can be define by.

$$n_j(E) = \frac{\int 2 \sum_{\mu,\mu'=-\frac{N}{2}}^{\frac{N}{2}-1} \sum_{i=-\frac{U}{2}}^{\frac{U}{2}-1} \delta[E - \{E^c_{\mu'}(k_i) - E^v_\mu(k_i)\}]dk_i}{\int \sum_{\mu,\mu'=-\frac{N}{2}}^{\frac{N}{2}-1} \sum_{i=-\frac{U}{2}}^{\frac{U}{2}-1} \delta[E' - \{E^c_{\mu'}(k_i) - E^v_\mu(k_i)\}]dk_i}. \tag{2.81}$$

The concept of JDOS is important in interband (valence band to conduction band) transition when the incident light energy is equal to the energy difference between the valance band and conduction band at a certain k point. In X-ray absorption, we generally use the DOS or partial density of states (PDOS) of unoccupied band because the core electronic band has a small (almost flat) energy dispersion. σ^* states are mixed of 2s, $2p_x$ and $2p_y$ orbital. So the total density of states of σ bands is contributed by PDOS of 2s, $2p_x$ and $2p_y$ orbitals. Specially in case of 1s to σ^* on

site transition, only $2p_x$ and $2p_y$ density of states contribute and 2s PDOS does not contribute to DOS because D^{fi} is odd function of x, y and z. The total density of states for all orbitals can be expresses as,

$$\begin{aligned}\rho(E) &= \sum_{i=2s,2p_x,2p_y} \rho_i(E), \\ &= \int \mid \Psi(\vec{k},\vec{r}) \mid^2 \delta(E - E(\vec{k}))d\vec{k}, \\ &= \int \sum_{i,j} C_i^*(\vec{k})C_j^*(\vec{k})\langle\Phi(\vec{k},\vec{r}) \mid \Phi(\vec{k},\vec{r})\rangle\delta(E - E(\vec{k}))d\vec{k} \end{aligned} \tag{2.82}$$

Where for σ band i and j stands for 2s, $2p_x$ and $2p_y$, $\rho_i(E)$ is the PDOS at energy E for i type orbital, $\rho(E)$ is the total denstiy of states (DOS),

$$\begin{aligned}\Psi^\sigma(\vec{k}) =& C_A^{2s}(\vec{k})\Phi_A(\vec{k},\vec{r}) + C_A^{2p_x}(\vec{k})\Phi_A(\vec{k},\vec{r}) \\ &+ C_A^{2p_y}(\vec{k})\Phi_A(\vec{k},\vec{r}) + C_B^{2s}(\vec{k})\Phi_B(\vec{k},\vec{r}) \\ &+ C_B^{2p_x}(\vec{k})\Phi_B(\vec{k},\vec{r}) + C_A^{2p_y}(\vec{k})\Phi_A(\vec{k},\vec{r}). \end{aligned} \tag{2.83}$$

Then partial density of states (PDOS) for i-type orbital is,

$$\begin{aligned}\rho_i(E) =& \mid \Psi(k,r) \mid^2 \\ &= \int_E \sum_j C_i^*(k)C_j(k)\langle\Phi(\vec{k},\vec{r}) \mid \Phi(\vec{k},\vec{r})\rangle\delta(E - E(k))dk. \end{aligned} \tag{2.84}$$

For example, we can write explicitly the PDOS for $2p_x$ of A atom,

$$\begin{aligned}\rho_A^{2p_x}(E) = \int_E \{& C_A^{2p_x{}^*}(\vec{k})C_A^{2p_x}(\vec{k})\langle\Phi_A^{2p_x}(\vec{k},\vec{r}) \mid \Phi_A^{2p_x}(\vec{k},\vec{r})\rangle \\ &+ C_A^{2p_x{}^*}(\vec{k})C_B^{2s}(\vec{k})\langle\Phi_A^{2p_x}(\vec{k},\vec{r}) \mid \Phi_B^{2s}(\vec{k_i},\vec{r})\rangle \\ &+ C_A^{2p_x{}^*}(\vec{k})C_A^{2p_y}(\vec{k})\langle\Phi_A^{2p_x}(\vec{k},\vec{r}) \mid \Phi_A^{2p_y}(\vec{k},\vec{r})\rangle \\ &+ C_A^{2p_x{}^*}(\vec{k})C_B^{2p_y}(\vec{k})\langle\Phi_A^{2p_x}(\vec{k},\vec{r}) \mid \Phi_B^{2p_y}(\vec{k},\vec{r})\rangle\}\delta(E - E(k))dk. \end{aligned} \tag{2.85}$$

Similarly we can calculate the PDOS for $2p_x$ of B atom.

$$\begin{aligned}\rho_A^{2p_x}(E) = \int_E \{ & C_B^{2p_x{}^*}(\vec{k}) C_A^{2p_x}(\vec{k}) \langle \Phi_A^{2p_x}(\vec{k},\vec{r}) \mid \Phi_A^{2p_x}(\vec{k},r)\rangle \\ & + C_B^{2p_x{}^*}(\vec{k}) C_B^{2s}(\vec{k}) \langle \Phi_A^{2p_x}(\vec{k},\vec{r}) \mid \Phi_B^{2s}(\vec{k_i},r)\rangle \\ & + C_B^{2p_x{}^*}(\vec{k}) C_A^{2p_y}(\vec{k}) \langle \Phi_A^{2p_x}(\vec{k},\vec{r}) \mid \Phi_A^{2p_y}(\vec{k},r)\rangle \\ & + C_B^{2p_x{}^*}(\vec{k}) C_B^{2p_y}(\vec{k}) \langle \Phi_A^{2p_x}(\vec{k},\vec{r}) \mid \Phi_B^{2p_y}(\vec{k},r)\rangle \} \delta(E - E(K)) dk. \end{aligned} \tag{2.86}$$

2.3.5 Gaussian line shape as an atomic orbital

Atomic orbital can be expressed as a summation of Gaussian function with amplitude I_k and Gaussian width σ_k. Using non linear fitting method, we can fit such Gaussian function with *ab-intio* calculation to find the fitting parameter I_k and σ_k with index k. The functional form of gaussian for $2p_z$ atomic orbital can be expressed as,

$$\phi(r) = z \frac{1}{\sqrt{N}} \sum_{k=1}^{n} I_k \exp\left\{\frac{-r^2}{2\sigma_k^2}\right\} \tag{2.87}$$

The radial part of the atomic orital can be expressd as,

$$f(r) = \frac{1}{\sqrt{N}} \sum_{k=1}^{n} I_k \exp\left\{\frac{-r^2}{2{\sigma_k}^2}\right\}. \tag{2.88}$$

Where z is the angular part of orbital wave function. N is the normalization constant, n is number of the Gaussian functions. Same functional form of Gaussian can be chosen for 1s and 2s atomic orbital except the angular part because 1s and 2s orbitals are spherially symmetric. The nomalization constant for 2p ($2p_x$,$2p_y$ and $2p_z$) orbital can be given by,

$$N_{2p} = \frac{\sqrt{8\pi^3}}{3} \sum_{l=1,k=1}^{n} \frac{1}{(\frac{1}{\sigma_k^2} + \frac{1}{\sigma_l^2})^{\frac{3}{2}}}. \tag{2.89}$$

The nomalization constant for 1s and 2s orbitalS can be given by,

$$N_s = \sqrt{8\pi^3} \sum_{l=1,k=1}^{n} \frac{1}{(\frac{1}{\sigma_k^2} + \frac{1}{\sigma_l^2})^{\frac{3}{2}}}. \tag{2.90}$$

The fitting parameters for 1s, 2s and 2p orbitals given in the table below.

Table 2.2: Fitting parameters of 1s orbital

I_k	7.7513	11.61669	6.04298	1.92502
σ_k	0.28	0.11206	0.03510	0.00665

Table 2.3: Fitting parameters of 2s orbital

I_k	-0.95773	2.75838	0.94915	3.53458
σ_k	-1.36189	0.07458	-0.01434	-0.23196

Table 2.4: Fitting parameters of 2p orbital

I_k	0.25145	0.76498	-0.67498	3.53458
σ_k	2.2532	1.03192	0.14805	0.02893

2.3.6 Atomic matrix element

The on-site and off-site atomic matrix elements for X-ray absorption process is calculated anlaytically by using Gaussian fucntion. Let us first derive the analytical expression for on-site atomic matrix elements. As an example, we will here consider that electron excited from 1s core orbital to the $2p_z$ orbital of same atom. The atomic matrix element can be expressed as,

$$\begin{aligned} m_{\text{opt}}^{\text{on}} &= \langle \phi^{2p_z}(r) \mid \nabla \mid \phi^{1s}(r) \rangle \\ &= \langle \cos\theta \mathrm{f}^{2p_z}(\mathrm{r}) \mid \nabla \mid \mathrm{f}^{1s}(\mathrm{r}) \rangle \end{aligned} \tag{2.91}$$

Where ∇ can be represented in the cartesian coordinate,

$$\nabla = \hat{i}\frac{\delta}{\delta x} + \hat{j}\frac{\delta}{\delta y} + \hat{k}\frac{\delta}{\delta z} \tag{2.92}$$

The radial part of atomic orbital wave function of 1s and $2p_z$ can be expressed as,

$$f^{1s}(r) = \sum_l I_l \exp[-\frac{x^2+y^2+z^2}{2\sigma_l^2}], \tag{2.93}$$

$$f^{2p_z}(r) = \sum_k I_k \exp[-\frac{x^2+y^2+z^2}{2\sigma_k^2}]. \tag{2.94}$$

When we operate ∇ on 1s orbital radial wave function, the integral of Eq. (2.91) is an odd function of x and y and even function of z. Thus, we can express the on-site matrix element as,

$$m_{\text{opt}}^{\text{on}} = \langle z f^{2p_z}(r) \mid \hat{k}\frac{\delta}{\delta z} \mid f^{1s}(r)\rangle \tag{2.95}$$

Therefore, the atomic dipole vector for $1s$ to $2p_z$ on site transition is directed in the $2p_z$ orbital direction. Now the amplitude of this vector can be obtain by differentiating the radial part of 1s wave function with respect to z and multiply it by atomic orbital wave function of $2p_z$. We can now integrate this integrand in the spherical polar coordinate. We obtain,

$$\begin{aligned} m_{\text{opt}}^{\text{on}} &= \sum_{k,l} I_k I_l \frac{1}{\sigma_l^2} \int r^3 \exp[-\frac{r^2}{2}(\frac{1}{\sigma_k^2}+\frac{1}{\sigma_l^2})] \int_o^{\pi} \cos^2\theta \sin\theta d\theta \int_0^{2\pi} d\varphi, \\ &= \sum_{k,l} I_k I_l \frac{8\pi}{3\sigma_l^2} \frac{1}{(\frac{1}{\sigma_k^2}+\frac{1}{\sigma_l^2})^2}. \end{aligned} \tag{2.96}$$

After putting the fitting parameters I_l,I_k,σ_k, σ_l in the Eq. (2.96) and using normalization factor from Eq. (2.89), Eq. (2.90) we obtain,

$$m_{\text{opt}}^{\text{on}} = 0.30[\text{a.u}]^{-1} \tag{2.97}$$

Where [a.u] is the atomic unit in which $1[a.u]^{-1} = 0.529$Å, Similarly, we can calculate the atomic matrix element for 1s to $2p_x$ and 1s to $2p_y$ on-site transition. The σ^* final state is a linear combination of 2s, $2p_x$ ad $2p_y$ orbitals. The atomic dipole vector directed along the x and y direction if the final state is $2p_x$ and $2p_y$, and amplitude of

the matrix element is $0.30[\text{a.u}]^{-1}$, because the atomic matrix element is odd function of y and z and even function of x when the final state is 2p_x. We can then also calculate for the case that the final state is 2p_y. The 1s to 2s on-site atomic martix element is vanish because the matrix element is odd function of x , y and z.

The off-site atomic martix element $m_{\text{opt}}^{\text{off}}$ can be calculated by expressing the atomic orbitals as a summation Gaussians. This numerical value is important to decide the contribution from off-site and on-site interaction in X-ray absorption process on graphene. Now let us consider the off-site X-ray absorption process. The $\phi^{2\text{p}_\text{z}}$ and $\phi^{1\text{s}}$ are wave function for two atom located on the xy plane. The distance between two atom is a_o=2.712[a.u]. For 1s to π^* transition the off-site matrix element is an even function of z and odd function of x and y. Then the atomic dipole vector for off-site transtion is directed along the z direction.

$$\begin{aligned} m_{\text{opt}}^{\text{off}} &= \langle \phi^{2\text{p}_\text{z}}(r) \mid \frac{\delta}{\delta z} \mid \phi^{1s}(r) \rangle \\ &= \langle \cos\theta f^{2\text{p}_\text{z}}(r) \mid \frac{\delta}{\delta z} \mid \phi^{1\text{s}}(r) \rangle \end{aligned} \tag{2.98}$$

The distance of the two atoms from the origin is α and β such that $\beta = -(a_0 - \alpha)$ as shown in Fig. 2-7. 1s orbital is spherically symmetric and the 2p_z orbital has both the radial part and the angular part of the wave function. The radial part of the wave function can be written as the summation of Gaussians,

$$f^{1\text{s}}(r) = \sum_l I_l \exp[\frac{-(x-\alpha_{kl})^2 - y^2 - z^2}{2\sigma_l^2}], \tag{2.99}$$

$$f^{2\text{p}_\text{z}}(r) = \sum_k I_k \exp[\frac{-(x+(a_o-\alpha_{kl}))^2 - y^2 - z^2}{2\sigma_k^2}]. \tag{2.100}$$

$\frac{\delta}{\delta z}$ will now act on $f^{1s}(r)$

$$\frac{\delta}{\delta z} f^{1\text{s}}(r) = -\sum_l I_l \exp[\frac{-(x-\alpha_{kl})^2 - y^2 - z^2}{2\sigma_l^2}] \frac{2z}{2\sigma_l^2}, \tag{2.101}$$

putting Eq. (2.101) in Eq. (2.98), we get

$$
\begin{aligned}
m_{\text{opt}}^{\text{off}} &= \sum_{k,l} I_k I_l \int \cos\theta \exp[\frac{-(x+(a_o-\alpha_{kl}))^2 - y^2 - z^2}{2\sigma_k^2}] \frac{z}{\sigma_l^2} \exp[\frac{-(x-\alpha_{kl})^2 - y^2 - z^2}{2\sigma_l^2}], \\
&= \sum_{k,l} I_k I_l \frac{1}{\sigma_l^2} \exp[\frac{-(a_o-\alpha_{kl})^2}{2\sigma_k^2}] \exp[-\frac{\alpha_{kl}^2}{2\sigma_l}] \int z\cos\theta \\
&\quad \times \exp[-\frac{r^2}{2}(\frac{1}{\sigma_k^2} + \frac{1}{\sigma_l^2})] \exp[x(\frac{\alpha_{kl}}{\sigma_l^2} - \frac{a_o-\alpha_{kl}}{\sigma_k^2})] dv. \qquad (2.102)
\end{aligned}
$$

We chose a special value of α_{kl} that one exponential function in the integral disappears. The condition is given by. $\frac{\alpha_{kl}}{\sigma_l^2} - \frac{a_o - \alpha_{kl}}{\sigma_k^2} = 0$ and thus $\alpha_{kl} = \frac{\frac{a_o}{\sigma_k^2}}{\frac{1}{\sigma_l^2} + \frac{1}{\sigma_k^2}}$ Using the α_{kl}, the integration over the exponential function disappear. Now let us

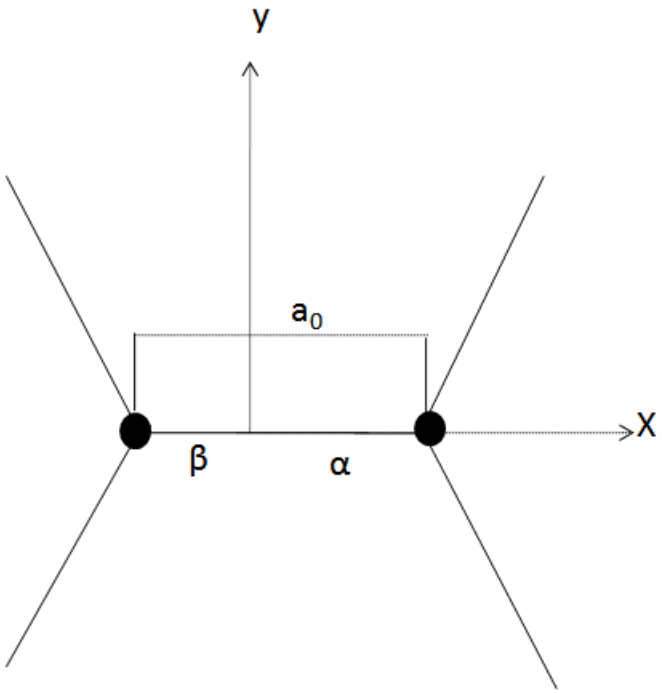

Figure 2-7: The coordinate used to calculate the off-site atomic matrix element. α and β are the distance of the two atoms from the origin. Radial part of the wave function are expressed as a function of distance from the atom.

use the spherical polar coordinates.

$$x = r\sin\theta\cos\varphi,$$
$$y = r\sin\theta\sin\varphi,$$
$$z = r\cos\theta,$$
$$dv = r^2\sin\theta d\theta d\varphi.$$

We can now get,

$$\begin{aligned} m_{\text{opt}}^{\text{off}} &= \sum_{k,l} I_k I_l \frac{1}{\sigma_l^2}\exp[\frac{-(a_o-\alpha_{kl})^2}{2\sigma_k^2}]\exp[-\frac{\alpha_{kl}^2}{2\sigma_l}]\int\cos\theta\exp[-\frac{r^2}{2}(\frac{z}{\sigma_k^2}+\frac{1}{\sigma_l^2})]dv, \\ &= \sum_{k,l} I_k I_l \frac{1}{\sigma_l^2}\exp[\frac{-(a_o-\alpha_{kl})^2}{2\sigma_k^2}]\exp[-\frac{\alpha_{kl}^2}{2\sigma_l}] \\ &\quad\times\int r^3\exp[-\frac{r^2}{2}(\frac{1}{\sigma_k^2}+\frac{1}{\sigma_l^2})]\int_o^{\pi}\cos^2\theta\sin\theta d\theta\int_0^{2\pi}d\varphi, \\ &= \sum_{k,l} I_k I_l \frac{8\pi}{3\sigma_l^2}\exp[\frac{-(a_o-\alpha_{kl})^2}{2\sigma_k^2}]\exp[-\frac{\alpha_{kl}^2}{2\sigma_l}]\frac{1}{(\frac{1}{\sigma_k^2}+\frac{1}{\sigma_l^2})^2}. \end{aligned} \tag{2.103}$$

Using the fitting parameter I_k, and σ_k for 1s and $2p_z$ atomic orbital we can calculate the atomic dipole matrix element. The result is 5.2×10^{-2} in unit of $[\text{at.u}]^{-1}$. The same anlaytical expression as in Eq. (2.104) can be used as the atomic matrix element for $1s$ to $2p_x$ and 1s to $2p_y$ off-site transtion. The corresponding dipole vector is along x and y direction respectively. Analytical expression for 1s to 2s off-site matrix element can be expressed

$$m_{\text{opt}}^{\text{off}} = \sum_{k,l} I_k I_l \frac{\alpha_{kl}\sqrt{8\pi^3}}{\sigma_l^2}\exp[\frac{-(a_o-\alpha_{kl})^2}{2\sigma_k^2}]\exp[-\frac{\alpha_{kl}^2}{2\sigma_l^2}]\frac{1}{(\frac{1}{\sigma_k^2}+\frac{1}{\sigma_l^2})^{3/2}}. \tag{2.104}$$

The atomic dipole moment is acting on the x direction.

2.3.7 Plane wave approximation

In the simple tight binding (STB) calculation we used the atomic orbitals as basis function and low energy band structure can be calculated satisfactorily. But if we

want to excite electron to more higher energy state, such high energy bands; in the case of graphene usually these are usually σ^* bands cannot be obtained by localised atomic orbitals. Therefore, σ^* states can be expressed as a summation of plane waves. Let us give an analytical expression for dipole vector for such plane wave final state. The 1s electron wave function in graphene can be expressed as Bloch fucntion

$$\Psi_i(\vec{k},\vec{r}) = C_A(k)\phi_A(k,r) + C_B(k)\phi_B(k,r) \tag{2.105}$$

where ϕ_A and ϕ_B is the Bloch fucntion.

$$\Phi(k,r) = \frac{1}{\sqrt{N}} \sum_N \exp[-i\vec{k}\cdot\vec{R}\varphi(\vec{r}-\vec{R}) \tag{2.106}$$

where graphene unit cell has two atoms A and B. N is the number of unit cell. Each atom has one 1s orbital. ϕ_A, and ϕ_B represent the Bloch orbitals for 1s electron. The final state can be epressed as summation of plane waves,

$$\Psi_f(\vec{k},\vec{r}) = \sum_G C_G \exp[i(\vec{k}+\vec{G})\cdot\vec{r}] \tag{2.107}$$

Where, G is the reciprocal translation vector, C_G is the wave function coefficient. We can now write the dipole vector $D^{fi}(\vec{k})$,

$$D^{if}(\vec{k'},k) = \langle \Psi^i(\vec{k'},\vec{r}) \mid \nabla \mid \Psi^f(\vec{k},\vec{r})\rangle \tag{2.108}$$

Putting Eqs. (2.105) and (2.107) to Eq. (2.108), we get,

$$\begin{aligned}
D^{if}(\vec{k'},k) =&\langle C_A(\vec{k'})\phi_A(\vec{k'},\vec{r}) + C_B(\vec{k'})\phi_B(\vec{k'},\vec{r}) \mid \nabla \mid \sum_{\vec{G}} C_{\vec{G}} \exp[i(\vec{k}+\vec{G}).\vec{r}]\rangle \\
=&\langle C_A(\vec{k'})\phi_A(\vec{k'},\vec{r}) \mid \nabla \mid \sum_{\vec{G}} C_{\vec{G}} \exp[i(\vec{k}+\vec{G}).\vec{r}]\rangle \\
&+ \langle C_B(\vec{k'})\phi_B(\vec{k'},\vec{r}) \mid \nabla \mid \sum_{\vec{G}} C_{\vec{G}} \exp[i(\vec{k}+\vec{G}).\vec{r}]\rangle \\
=&\langle C_A(\vec{k'})\phi_A(\vec{k'},\vec{r}) \mid \nabla \mid \sum_{\vec{G}} C_{\vec{G}} \exp[i(\vec{k}+\vec{G})\cdot(\vec{r}-\vec{R}+\vec{R})] \\
&+ \langle C_B(\vec{k'})\phi_B(\vec{k'},\vec{r}) \mid \nabla \mid \sum_{\vec{G}} C_{\vec{G}} \exp[i(\vec{k}+\vec{G})\cdot(\vec{r}-\vec{R}+\vec{R})]
\end{aligned} \tag{2.109}$$

Let us now consider the transition from A atom, since the two part are same.

$$\begin{aligned}
D^{if}(\vec{k'},k) =&C_A(\vec{k'}) \sum_G C_G \langle \exp[-i\vec{k'}.\vec{R}]\varphi(\vec{r}-\vec{R}) \mid \nabla \mid \exp[i(\vec{k}+\vec{G})\cdot(\vec{r}-\vec{R}+\vec{R})] \\
=&C_A(\vec{k'}) \sum_{\vec{G}} C_{\vec{G}} \langle \exp[-i\vec{k'}.\vec{R}]\varphi(\vec{r}-\vec{R}) \mid \nabla \mid \\
&\exp[i(\vec{k}+\vec{G})\cdot\vec{R})] \exp[i(\vec{k}+\vec{G})\cdot(\vec{r}-\vec{R})]\rangle \\
=&C_A(\vec{k'}) \sum_{\vec{G}} C_{\vec{G}} \exp[-i(\vec{k'}-\vec{k}).\vec{R}] \exp[i(\vec{k}+\vec{G})\cdot\vec{R}] \\
&\langle \varphi(\vec{r}-\vec{R}) \mid \frac{d}{d(\vec{r}-\vec{R})} \mid \exp[i(\vec{k}+\vec{G})\cdot(\vec{r}-R)]\rangle \\
=&C_A(\vec{k'}) \sum_{\vec{G}} C_{\vec{G}} \delta_{k',k} 2\pi \langle \varphi(\vec{r}-\vec{R}) \mid \frac{d}{d(\vec{r}-\vec{R})} \mid \exp[i(\vec{k}+\vec{G})\cdot(\vec{r}-R)]\rangle \\
=&C_A(\vec{k'}) \sum_{\vec{G}} C_{\vec{G}} 2\pi \delta_{k',k} i(\vec{k}+\vec{G}) \int \varphi(\vec{r}-\vec{R}) \exp[i(\vec{k}+\vec{G})\cdot(\vec{r}-R)] d(\vec{r}-R) \\
=&C_A(\vec{k'}) \sum_{\vec{G}} C_{\vec{G}} 2\pi \delta_{k',k} i(\vec{k}+\vec{G}) \varphi(\vec{k}+\vec{G})
\end{aligned} \tag{2.110}$$

Here $\varphi(\vec{k}+\vec{G})$ is the Fourier transfomation of atomic orbital $\varphi(r)$ Let us consider

$$\vec{k}+\vec{G}=\vec{q} \tag{2.111}$$

Then we can write

$$D^{fi}(\vec{k'},k)=C_A(\vec{k'})\sum_{\vec{G}} C_{\vec{G}} 2\pi\delta_{k',k} i\vec{q}\varphi(\vec{q}) \tag{2.112}$$

Then matrix element for such a transition due to a X-ray incident beam can be expressed as

$$\begin{aligned} M(\vec{k'},k) =& P\cdot D^{fi}(\vec{k'},k) \\ =& C(\vec{k'})\sum_{G} C_{\vec{G}} 2\pi\delta_{k\vec{'},k} i(\vec{P}\cdot\vec{q})\varphi(\vec{q}) \end{aligned} \tag{2.113}$$

Here P is the polarization veector of the incident X-ray beam. Square of the matrix element $M(k)$ will give the probability of absorption. Absorption intensity I(k',k)in the reciprocal space can be expressed as

$$I(k',k) =\mid M(k',k)\mid^2 =[2\pi]^2 \mid \sum_{\vec{G}} C_{\vec{G}} C(\vec{k'})\vec{P}\cdot\vec{q}\varphi(\vec{q})\mid^2 \tag{2.114}$$

Therefore, absorption intensity can be writen as a function of energy if we integrate Eq. (2.114) along the equi energy contour line in the reciprocal space as,

$$\begin{aligned} I(E) =& \int \mid M(k',k)\mid^2 \delta(E(k)-E(k')-E)dk \\ =& \int [2\pi]^2 \mid \sum_{\vec{G}} C_{\vec{G}} C(\vec{k'})\vec{P}\cdot\vec{q}\varphi(\vec{q})\mid^2 \delta(E(k)-E(k')-E)d\vec{k} \end{aligned} \tag{2.115}$$

Where the integration taken over the Brilloin zone. The transtion probability $W(k)$ from $1s$ energy level to a higher unoccupied σ^* state at energy $\hbar\omega$ which is given by Fermi golden rule can be expressed as,

$$W(k',k) = [2\pi]^2 \mid \sum_{\vec{G}} C_{\vec{G}} C(\vec{k'}) \vec{P} \cdot \vec{q} \varphi(\vec{q}) \mid^2 \delta \left[\frac{\hbar^2(\vec{k}+\vec{G})^2}{2\mathrm{m}} - E_{1s}(k') - E_x \right] \quad (2.116)$$

Where $E_{1s}(\vec{k'})$ is the $1s$ core electron band, $\frac{\hbar^2(\vec{k}+\vec{G}^2}{2m})$ gives the final state band, E_x is the incident X-ray energy. The δ function select X-ray absoprtion along the corresponding equi energy contour line. Let us calculate $\varphi(q)$

$$\begin{aligned} \varphi(\vec{q}) &= \int \varphi(\vec{r}) \exp[i(\vec{k}+\vec{G}) \cdot \vec{r}] d(\vec{r}) \\ &= \int \varphi(r) \exp[iqr\cos\theta] \mathrm{r}^2 \sin^2\theta \mathrm{d}\theta \mathrm{d}\phi \end{aligned} \quad (2.117)$$

$\varphi(r)$ is the intial state 1s atomic orbital wave function that can be expressed as the summation of Gaussian line shape that we already described in Eq. (2.94). Now we can write,

$$\varphi(\vec{q}) = \int [\sum_i a_i \exp\left[-\frac{r^2}{2\mathrm{b_i^2}}\right] \exp[i\mathrm{qr}\cos\theta] \mathrm{r}^2 \sin\theta \mathrm{dr} \mathrm{d}\theta \mathrm{d}\phi \quad (2.118)$$

Where a and b are the amplitude and width of the Gaussian fucntion of atomic orbital in real space. After doing the integration over r,θ and ϕ, we can write,

$$\varphi(\vec{q}) = 4\pi\sqrt{\frac{\pi}{2}} \sum_i \mathrm{a_i b_i^3} \exp\left[-\frac{\mathrm{b_i^2 q^2}}{2}\right] \quad (2.119)$$

Where $\varphi(\vec{q})$ is a Gaussian function which is the Fourier transform of the intial 1s state atomic orbital $\varphi(r)$. We remembered that $\varphi(\vec{r})$ is the atomic orbital wave function of initial state. This orbital is very localised in the real space. It is possible to calculate X-ray absorption spectra by using plane wave as final state if the wave function coefficient of plane wave C_G is given. C_G can be calculated first principle calculation.

Chapter 3

Results and discussion

In this chapter, we describe the original results of the thesis.

3.1 Atomic Matrix element

We show in chapter 2 that the dipole vector $\vec{D}(\vec{k}_i, \vec{k}_f)$ is related to 1s to π^* transtion or 1s to σ^* transition, which is consist of on-site and off-site atomic matrix element. Here we first calculate the atomic matrix elements related to on-site transition and off-site transition. The calculated numerical values of matrix elements are important because such values determine the optical transitions quantitatively.

3.1.1 On-site and off-site interaction

The radial part of the atomic wave function of 1s, 2s and 2p orbitals are expressed as the summation of Gaussian functions in Eq. (2.88). These Gaussian functions are fit to *ab-initio* calculation by non-linear least square method of fitting. The fitting parameters are given in Table. 2.2, Table. 2.3 and Table. 2.4 for 1s, 2s and 2p atomic orbital, respectively. The atomic matrix element m_{opt} for 1s to π^* on-site transition is $0.30[\text{a.u}]^{-1}$ and the dipole vector related to this matrix element is odd function of x, y and z. For 1s to σ^* on-site transition, we get a matrix element from two in-plane orbitals, 2p_x and 2p_y. The atomic matrix elements due to these two orbitals

are 0.30[a.u]$^{-1}$ same as for 1s to π^*. Because of the $2p_x$ and $2p_y$ orbital symmetry, the dipole vector for 1s to σ^* on-site transition directed on the xy graphene basal plane. Although the 2s orbital is contributed to form σ orbital, the 2s orbital does not contribute to on-site transition beacuse the matrix element $\langle 2s \mid \nabla \mid 1s \rangle$ is an odd function of x, y or z. The atomic matrix element for 1s to π^* off-site transition is 5.2 $\times 10^{-2}$ [a.u]$^{-1}$. We have also calculated $1s$ to $2s$ off-site atomic matrix element which is -6.96$\times 10^{-}2$[a.u]$^{-1}$. The negative sign appears because there is a node in the radial wave function of the 2s orbital. Since the distance between the C-C atom is 2.71 a.u., wave function of 1s orbital of carbon atom quickly decreases with increasing the distance. Thus, the overlap between 1s to 2p orbitals ($2p_x$, $2p_y$, $2p_z$) is much weaker than that of π to π^* transition (0.21[a.u]$^{-1}$). On the other hand, beacuse of the same atomic position, the overlapping of the wave functions is not small even though $\langle 1s \mid 2s \rangle = 0$. By analysing the atomic matrix element, the direction of the dipole vector given by atomic dipole vector which is independent of k vector. The k dependent part appears from the wavefunction coefficient in case of the on-site interaction and the wave function coefficient and the phase factor in case of the off-site interaction. We will consider only the on-site transition to calculate the X-ray absortption spectra as a first approximation.

3.2 1s to π^* transition

The dipole vector for 1s to π^* on-site transtion is lies in the direction perpendicular to the graphene plane. The amplitude of the dipole vector $O = \sqrt{\vec{D}(\vec{k}_f, \vec{k}_i) \cdot \vec{D}(\vec{k}_f, \vec{k}_i)}$ which is called oscillator strength is shown in Fig. 3-1. From the Fig 3-1, it is clear that the oscillator strength is the maximum at the Γ point and that is minimum near the K points, which is the property of graphene for 1s to π^* transition. In the Fig. 3-2, we plot the equi-energy contour line as a function of (a) the intial wave vector $\vec{k}_i$ and (b) the final wave vector $\vec{k}_f$. We find that each equi-energy contour is larger in the Fig. 3-2(b). It is because, in case of the non-vertical transition, the final state contour line becomes relatively smaller than the initial state contour line to satisfy the energy

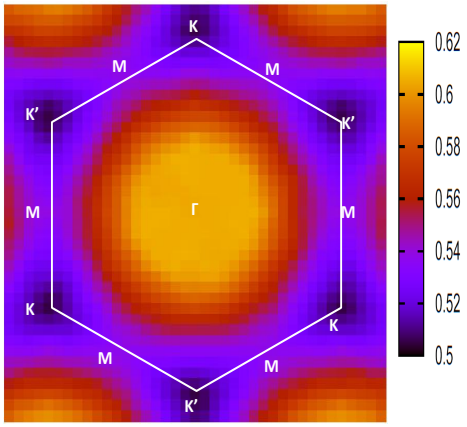

Figure 3-1: The oscillator strength in the unit of $m_{\rm opt}$ as a function of the final wave vector $\vec{k}_f$ in the 2D Brillouin zone. The bright color shows the strong oscillator strength, and the dark color shows the weak oscillator strength.

momentum conservation as shown in Fig. 3-2.

From the atomic matrix element calculation, we know that the dipole vector for 1s to π^* transition directed along the perpendicular to the graphene basal plane as shown Fig. 3-3(b). In Fig. 3-4, we plot the X-ray absorption intensity as a function of incident X-ray energy for $\alpha = 10$ to $50°$. If $\alpha = 90°$ the X-ray absoprtion intensity becomes the maximum since the polarization direction $\vec{P}$ and the dipole vector $\vec{D}$ are parallel to each other. At $\alpha = 0°$, no intensity is found because cosine of $90°$ is zero. The 1s to π^* transition peak is found at 286.4eV, which is approximately 1eV higher than the experimentaly observed value. In this calculation, we use a single particle DOS to calculate the X-ray absoprtion intensity. Thus, such 1eV difference between the calculated value and the observed value [8] can be attributed to the core-hole attraction (core exciton) which is beyond the scope of this thesis.

The peak intensity of 1s to π^* transition increased as the angle α increased. As the angle α increases, the angle between the dipole vector which is directed to the

Fig. 3-1: figure/dp_pz1.pdf
Fig. 3-2: figure/equ_pz.pdf
Fig. 3-3: figure/vec_sig.pdf
Fig. 3-4: figure/intn_pz_fn.pdf

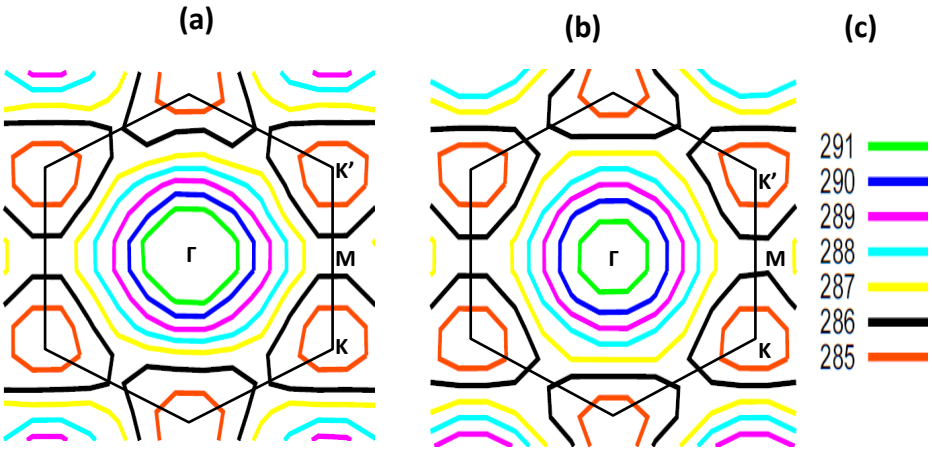

Figure 3-2: The equi energy contour line as a function of (a) the initial wave vector $\vec{k}_i$ and (b) the final wave vector $\vec{k}_f$ in the 2D Brillouin zone for 1s to π^* transition, (c) the color line number gives the energy in eV of corresponding equi energy contour line.

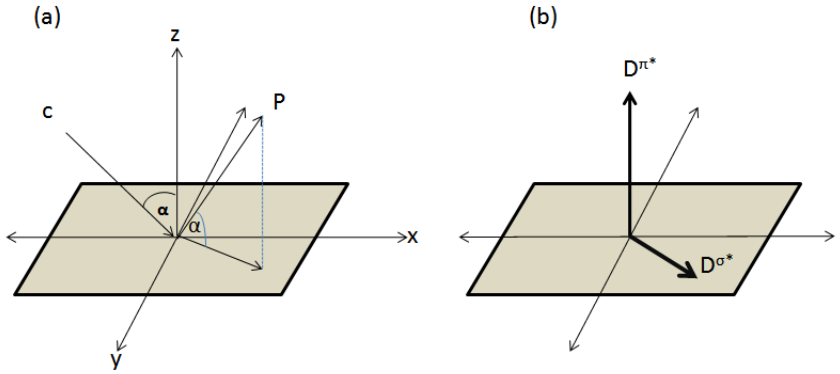

Figure 3-3: Directions of vectors. (a) c is the vector giving the direction of X-ray, P is the polarization direction which is perpendicular to the X-ray incident direction c. α is the angle between c and perpendicular direction of the graphene plane. α is also the angle between polarization vector P and xy plane (b) the dipole vector D^{π^*} for 1s to π^* is acting along the z direction. The dipole vector D^{σ^*} for 1s to σ^* transition is acting along the xy plane.

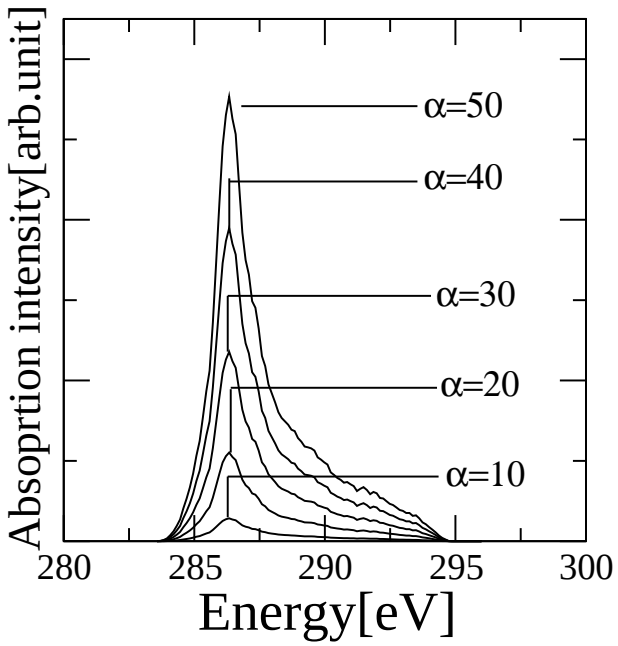

Figure 3-4: X-ray absorption intensity as a function of X-ray energy for 1s to π^* transition as various angles α.

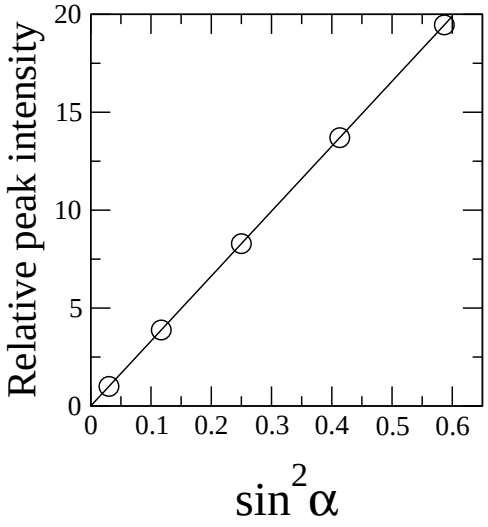

Figure 3-5: Relative peak intensity for 1s to π^* as a function of $\sin^2\alpha$.

z direction and the polarization unit vector decreases. Thus the matrix element $\mid \vec{P} \cdot \vec{D}(\vec{k}_f, \vec{k}_i) \mid^2$ is responsible for the angular dependence of intensity. Because of the square term in the matrix element, the peak intensity is proportional to the $\sin^2\alpha$ which is shown in Fig. 3-5.

Fig. 3-5: figure/pz_alpha.pdf

Now let us plot the X-ray absorption intensity in the 2D Brillouin zone as a function of the final wave vector $\vec{k}_f$ in Fig. 3-6. The incident energy is chosen as 286.4eV because as is given in Fig. 3-4, we found that 1s-π^* transition occur at 286.4eV. Even though the oscillator strength given in Fig. 3-1 around the K point and the M point is very small, but its not zero and we get strong X-ray absorption around the K points because many k points and thus a high DOS satisfy the energy momentum conservation along the M-M lines. The oscillator strength found maximum at the Γ point but the intensity is found zero at the Γ point because no k points at and near the Γ point satisfy the energy momentum consevation. That is, the multiplication between the δ-function and squared of the matrix element of Eq. (2.58) give the intensity distribution in the 2D Brillouin zone. When we increase the α from 30° to 60°, the intensity in the 2D Brilluin zone increases which is shown in Fig. 3-6(a) and Fig. 3-6(b) respectively. The value in color bar is shown in the unit of absorption intensity in $[\text{a.u}]^{-2}$. The position of the absorption location is not changed because the incident X-ray energy is fixed at 286.4eV. On the other hand, the intensity in the k space depend of the square matrix element which is angle dependent given in Eq. (2.58). Because of the perpendicular direction of the dipole vector corresponding to $1s - \pi^*$ transition, the intensity is directly proportional to $\sin^2\alpha$. In such a way, the polarization dependence of X-ray absorption spectra for 1s to π^* appears. When the X-ray energy is chosen to be 288eV, the X-ray absorption occur along the corresponding equi-energy contour line in the middle part of the 2D Brillouin zone as shown in Fig. 3-7. We have seen that the oscillator strength is relatively strong around the Γ point, but since the small number of k points and thus small DOS statisfy the energy momentum conservation at this energy. Thus, we get relatively small intensity at around the Γ point which is also confirmed from Fig. 3-4.

Fig. 3-6: figure/intnpz286.pdf
Fig. 3-7: figure/intnpz288.pdf

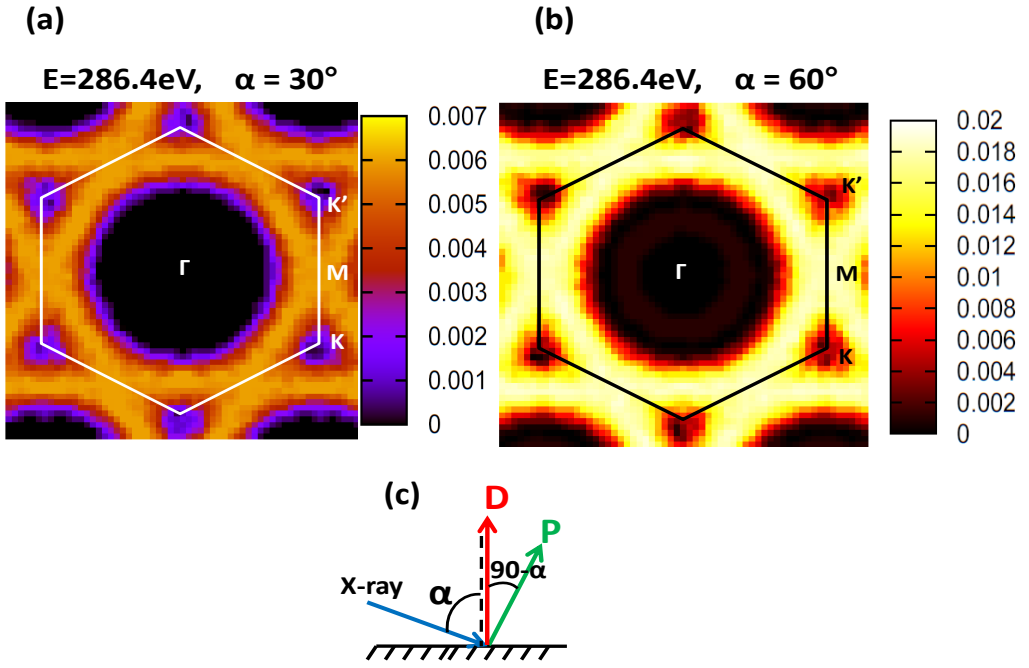

Figure 3-6: The X-ray absoprtion intensity (the bright area shows strong X-ray absorption and the dark area show weak X-ray absorption) of $1s$ to π^* transition as a function of the final wave vector $\vec{k}_f$ in the 2D Brillouin zone of graphene.(a) The X-ray energy $E = 286.4$eV, $\alpha = 30°$ and (b) The X-ray energy $E = 286.4$eV, $\alpha = 60°$. (c) the direction of the incident X-ray beam relative to graphene plane. The direction of the polarization vector P and the direction of the dipole vector D for $1s$ to π^* transtion are parallel to each other and P perpendicular to the graphene basal plane. The values in the color bar given in $[\text{a.u}]^{-2}$.

3.3 1s to σ^* transition

Let us consider the σ^* band in 2D graphene. In graphene, there are three sp^2 hybrid orbitals for one carbon atom made of 2s, $2p_x$ and $2p_y$ atomic orbitals. The orientation of the σ orbital lies in-plane. Since, there are two carbon atoms. Thus, we have six σ energy bands. Three of this six σ energy bands are occupied states called valence σ bands and other three bands are above the Fermi level called the unoccupied conduction σ^* bands. Among this three unoccupied σ^* bands, the first two are the lower energy σ^* bands and the peak for 1s to σ^* transition is belongs to these two low energy σ^* bands. The highest energy σ^* band which is obtained by the tight binding approximation has a clear energy band gap from the first two unoccupied σ^*

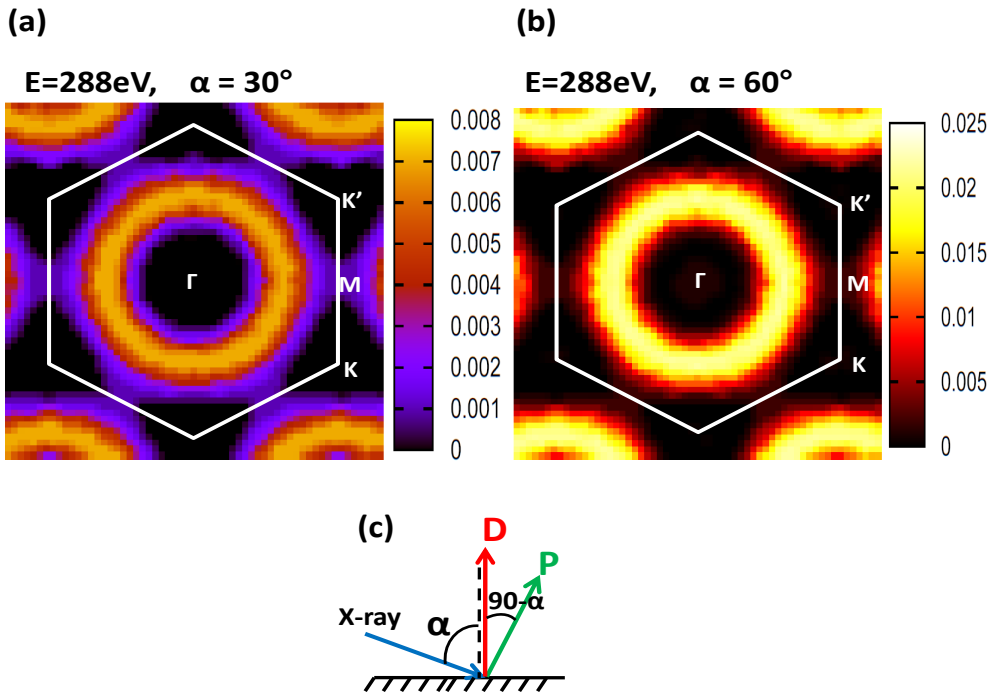

Figure 3-7: The X-ray absoprtion intensity (the bright area shows strong X-ray absorption and the dark area show weak X-ray absorption) of $1s$ to π^* transition as a function of the final wave vector $\vec{k}_f$ in the 2D Brillouin zone of graphene.(a) The X-ray energy $E = 288$eV. $\alpha = 30°$ and (b) The X-ray energy $E = 288$eV, $\alpha = 60°$. (c) the direction of the incident X-ray beam relative to graphene plane. The direction of the polarization vector P and the direction of the dipole vector D for $1s$ to π^* transtion are parallel to each other and P perpendicular to the graphene basal plane. The values in the color bar given in $[\text{a.u}]^{-2}$.

state. Because of the absence of DOS at around 293eV, the third σ^* band does not have contribution to the σ^* resonance peak around 293eV. The dipole vector for 1s to σ^* transtion is the summation of the atomic dipole vectors for $1s$ to 2s, $2p_x$ and $2p_y$ orbitals. We showed that the on-site dipole vector matrix element (Eq. 2.74) is larger than the off-site dipole vector matrix element (Eq. 2.75). Here we consider the dipole vector for on-site transition. Because of the odd function of x,y and z the dipole vector for $1s$ to 2s on-site transition vanish. Then the 1s to σ^* on-site transtion only consists of $1s$ to $2p_y$ and 1s to $2p_x$ transition. The dipole vector lies along x or y direction if the final states are $2p_x$ or $2p_y$ orbitals, respectively. Let us plot the dipole vector for transition from 1s to the two unoccupied lower energy σ^* bands. We named these two bands as σ_1^* and σ_2^*. The on-site dipole vectors for 1s to σ_1^* and to

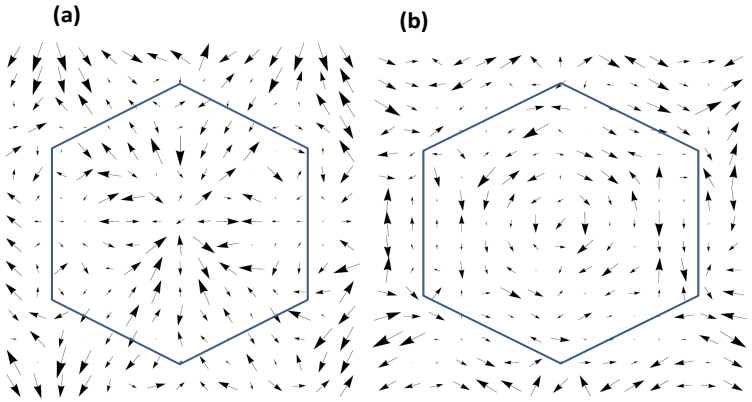

Figure 3-8: Dipole vector for (a)1s to σ_1^* transition and (b)1s to σ_2^* transition as a function of the final wave vector $\vec{k}_f$ in the 2D BZ.

σ_2^* are shown in Fig. 3-8(a) and Fig. 3-8(b), respectively.

If we closely look at Fig. 3-8(a), we observe that the dipole vector are radially inward to the Γ point. Now let us recall the dipole vector for 1s to σ^* on-site transition which can be written as

$$\vec{D}^{\text{on}}(\vec{k_f},\vec{k_i}) = C_A^{2\text{p}_\text{x}^*}(\vec{k_f})C_A^{1\text{s}}(\vec{k_i})m_{\text{opt}}^{AA}\hat{\vec{x}} + C_A^{2\text{p}_\text{y}^*}(\vec{k_f})C_A^{1\text{s}}(\vec{k_i})m_{\text{opt}}^{AA}\hat{\vec{y}} \tag{3.1}$$

The orientation of the dipole vector in the 2D Brillouin zone as a function of the final electron wave vector $\vec{k}_f$ given in Fig. 3-8 can be explained by the contribution of the final state orbital symmetry. According to Eq. (3.1), the dipole vectors completely align in the x or y direction give us the information about the corresponding final states 2p_x or 2p_y respectively which is given by the wavefucntion cofficient $C_A^{2\text{p}_\text{x}^*}(\vec{k_f})$ and $C_A^{2\text{p}_\text{y}^*}(\vec{k_f})$. There are other dipole vectors oriented in the xy plan have final state with mixed symmetry. Thus, the dipole vector can give the information about the final state symmetry in the 2D Brillouin zone. Since the dipole vectors for σ_1^* and σ_2^* are perpendicular to each other. Thus lower energy anti-bonding states have distinct

Fig. 3-8: figure/vecpisg.pdf

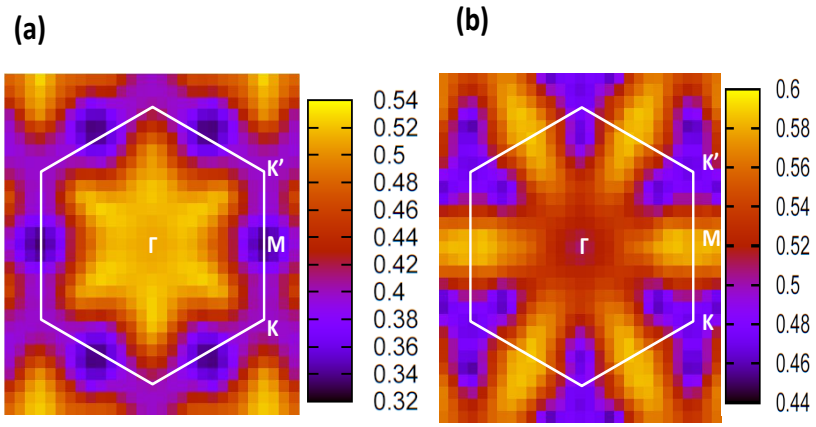

Figure 3-9: (a) Oscillator strength for 1s to σ_1^* on-site transition as a function of the final wave vector $\vec{k}_f$ in the 2D BZ and (b) oscillator strength for 1s to σ_2^* on-site transition as a function of final wave vector $\vec{k}_f$ in the 2D BZ. The bright area shows the strong oscillator strength and the dark area shows the weak oscillator strength. The number in the color bar is given in unit $m_{\rm opt}$. Here we use the on site atomic matrix element $m_{\rm opt} = 0.30[\text{a.u}]^{-1}$

symmetry which shows the atomic orbital nature of the final states.

In Fig. 3-9(a) and (b) we have plotted the amplitude of the corresponding dipole vector for 1s-σ_1^* and 1s-σ_2^* as a function of the final wave vector $\vec{k}_f$ respectiely. Fig. 3-9(a) shows that the oscillator strength is the minimum near the M point but it is not zero and the maximum near the Γ point. Near the K point we have also moderate oscillator strength for 1s to σ_1^* on-site transition. The oscillator strength for 1s to σ_2^* on-site transition is shown in Fig. 3-9(b). Fig. 3-9 shows that the maximum oscillator strength is found at the M point and the minimum oscillator strength is found at around the K point which is not zero.

Fig. 3-10 shows the X-ray absorption intensity for 1s to σ^* transition as a function

Fig. 3-9: figure/oscisg12.pdf

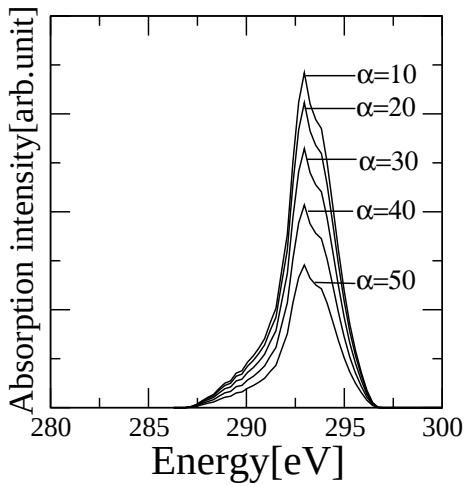

Figure 3-10: X-ray absorption intensity as function of incident X-ray energy at various angle α.

of incident X-ray energy at various angle α. Here by σ^*, we are considering the total contribution from σ_1^* band and σ_2^* band. The intensity increase with the decreasin angle, because the matrix element increase with decreasing the angle. When the angle $\alpha = 0$, the intensity should be the maximum and when the $\alpha = 90°$, the intensity become zero and there is no absorption peak, because at $\alpha = 90°$ the matrix element $\mid \vec{P}\cdot\vec{D}(\vec{k}_f, \vec{k}_i) \mid^2$ become zero. The 1s to σ^* resonance occur at 292.9eV which is around 0.5eV higher that of the experimental value which is reported by R.A Rosenberg *et al.* [8]. If we increase the angle α, then the k dependent, the square of the matrix element $|\vec{P}\cdot\vec{D}(\vec{k}_f, \vec{k}_i)|^2$ changes as function of $\cos^2\alpha$ and the summation of δ-function which gives the DOS.

Fig. 3-11 shows that the relative peak intensity increases with increasing the angle. The peak intensity of 1s to σ^* transition is linearly proportional to the $\cos^2\alpha$. The corresponding dipole vector for 1s to σ^* is directed along the graphene basal plane shown in Fig. 3-3 which is obtained from the atomic matrix element.

X-ray absorption spectra (XAS)is generally plotted as a function of incident X-ray energy. Then if we integrate Eq. (2.58) on a equi energy contour in the 2D BZ, we get the XAS as a function of energy. The expression for XAS is given in Eq. (2.60).

Fig. 3-10: figure/intn_sg_fn.pdf
Fig. 3-11: figure/sig_alpha1.pdf

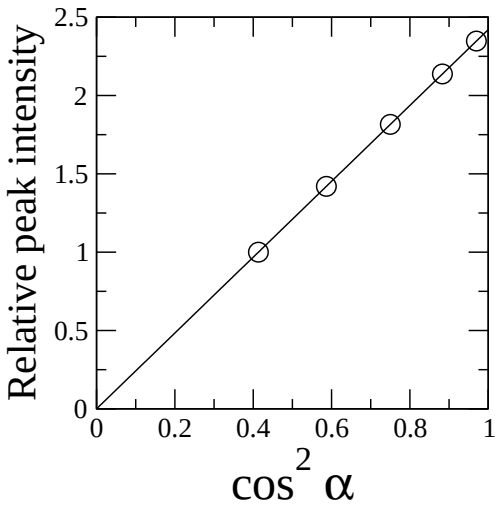

Figure 3-11: Relative peak intensity for 1s to σ^* as a function of $\cos^2\alpha$.

Thus, this equation has two parts; one is the absorption matrix element and the other is the density of states. The square of the matrix element $\mid \vec{P}\cdot\vec{D}(\vec{k}_f,\vec{k}_i)\mid^2$ is modified by the angle α, the angle between the polarization vector $\vec{P}$ and the dipole vector $\vec{D}$. The geometry of such X-ray absorption process is shown in Fig. 3-3.

Let us plot the XAS in the 2D BZ as function of the final wave vector in Fig. 3-12. Even though the oscillator strength for 1s-σ_1^* shown in Fig. 3-9(a) becomes the maximum near the Γ point, but the intensity is zero near the Γ ponit because the δ-function of Eq. 2.58 does not select any k points near the Γ point which satisfy energy momentum conservation for the incident X-ray energy 292.9eV. Thus, the multiplication of the oscillator strength and the δ-function gives the intensity distribution in the 2D BZ. In the case of 1s-σ_2^* transition, it is observed from Fig. 3-12 that intensity along the M point and near the Γ point is zero even though the corresponding oscillator strength shown in Fig. 3-9(b) shows moderate value near Γ point and even the maximum value at the M point as shown in Fig. 3-9(a).

Fig. 3-12: figure/intnsg293.pdf

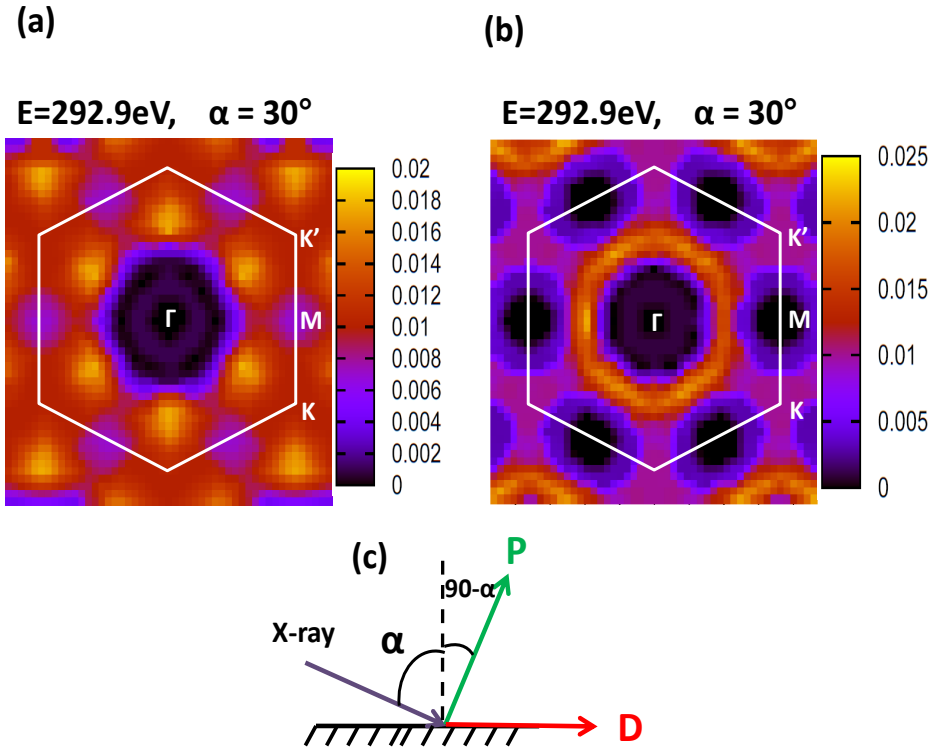

Figure 3-12: (a)The X-ray absoprtion intensity (the bright area shows strong X-ray absorption and the dark area show weak X-ray absorption) of 1s to σ_1^* transition as a function of the final electron wave vector in the 2D Brillouin zone of graphene. The X-ray energy $E = 292.9$eV, $\alpha = 30°$ and (b) The X-ray absoprtion of 1s to σ_2^* transition as a function of the final electron wave vector in the 2D Brillouin zone of graphene. The X-ray energy $E = 292.9$eV, $\alpha = 30°$. The direction of the polarization vector P and the direction of the dipole vector D for $1s$ to σ^* transtion which is act along the xy graphene basal plane. The values in the color bar given in [a.u]$^{-2}$.

3.4 JDOS and XAS spectra

The energy dispersion relation of π and σ bands of 2D graphene along the high symmetry direction and the joint density of states (JDOS) of 2D graphene are given in Fig. 3-13(a) and (b) respectively. The peak around 286.4eV in Fig. 3-13(a) corresponds to 1s-π^* transition peak and at around 293 eV correspond to so called 1s-σ^* transition peak which is mainly contributed by σ_1^* and σ_2^* band shown in Fig. 3-13(b). The third peak around 302eV is originated due to the σ_3^* band. If we want to compare the calculated JDOS with the experimental XAS spectra we must take into account

the angle dependent matrix element which is responsible for the polarization dependence of XAS spectra. As for example, at $\alpha = 0^\circ$ or at $\alpha = 90^\circ$, only the σ or π JDOS will appear in the XAS spectra. In Fig. 3-14(a) and (b), we have plotted the experimental XAS spectra and calculated XAS spectra respectively. From fig. 3-4 and Fig. 3-10, it is found that between 286.2eV to 295eV the X-ray absorption intensity is contributed by both π and σ band. This overlapping of XAS is not only due to energy dependent JDOS but also from angle dependent matrix elements. We have compared our calculated XAS spectra with the experimental XAS spectra at different angle α which is shown in Fig. 3-14. Two prominent peaks found at 286.4eV and 292.9eV obtained from our calculated XAS spectra by dashed line A and solid line B respectively which have π and σ^* symmetry. The calculated results show a reasonable agreement with the experimentally observed spectra except for the peak position which is found slightly higher than that of the experiment. At high energy region, a localized peak at 302eV is observed in Fig. 3-14(b)which is calculated by tight binding model. This high energy σ^* peak denoted by the solid line E is appear in the calculated XAS spectra because the localized atomic orbital is used to calulate the matrix element. Between 296.5 to 301eV, no XAS intensity is found in Fig. 3-14(b) becuase of the absence of DOS in this region. On the other hand, in the high energy region of the experimental XAS spectra in Fig. 3-14(a), wavy nature appears and then it is smoothly decreasing as a function of energy which is like free elctron DOS. The weak peak is observed around 302eV which is identified as a σ_3^* peak. Thus in the high energy region the tight binding approximation does not work satisfactorily because electronic states become more delocalized. Thus, in high energy region the electronic states should expressed in terms of the plane waves, which is discussed in the next section.

Fig. 3-13: figure/jdsxas1.pdf
Fig. 3-14: figure/comf1.pdf

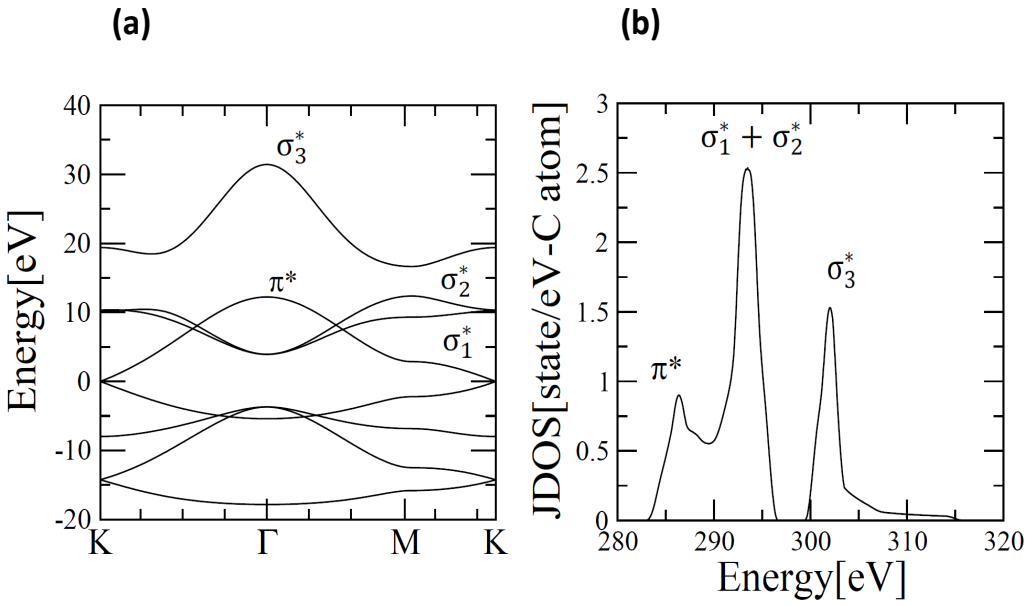

Figure 3-13: (a) The energy dispesion relation of π and σ bands of 2D graphene along the high symmetry direction, (b) The joint density of states (JDOS) of graphene as a function of energy. The JDOS from 1s orbitals to unoccupied states.

3.5 Plane wave approximation

Finally, we briefly discuss the preliminary results for transition from 1s to the unoccupied energy band whcih consist of plane waves. The high energy antibonding σ^* band can be obtained as the summation of plane waves, because such an electron in high energy state have a free electron nature. The final state has free-electron energy band character, and we expect that the transition from 1s to such free electron state is a non-vertical transition. The square of the absorption matrix element $M(\vec{k'}, \vec{k})$, which is given by Eq. (2.114) is proportional to the absoprtion intensity in the reciprocal space. Fig. 3-15(a) shows the absoprtion intensity for $\vec{G} = 0$ as a function of the final $\vec{k}$ vectors. The intensity found zero at Γ point or the center of the reciprocal space. As we move far from the Γ point we will find more high energy region which

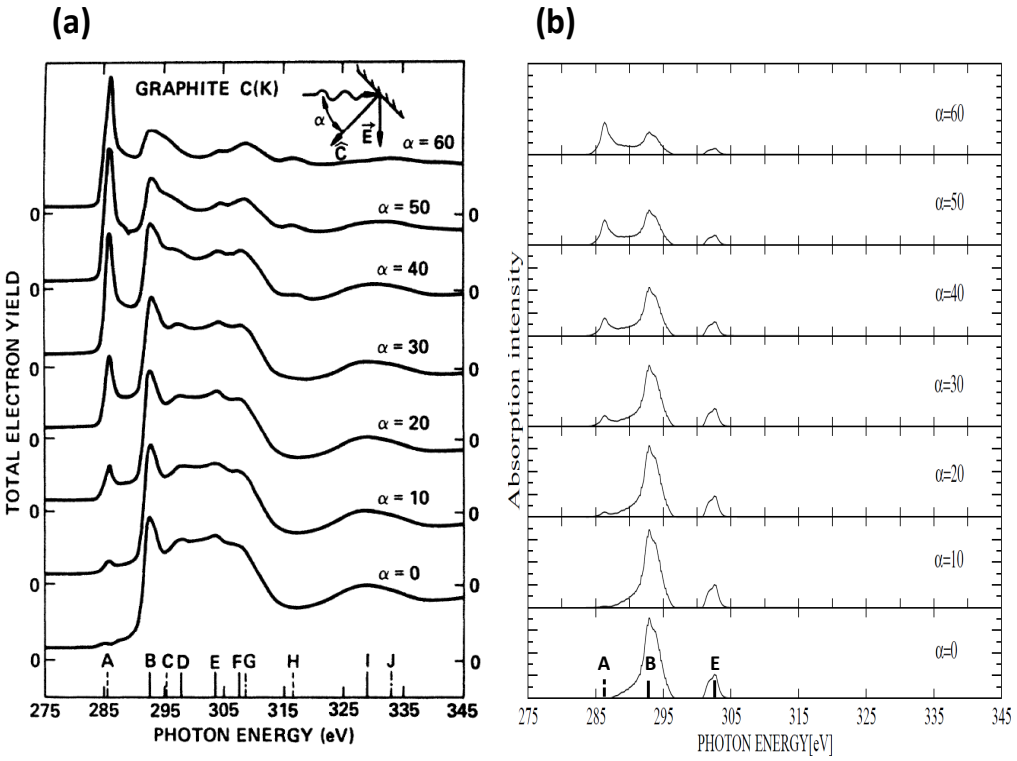

Figure 3-14: C(K)-edge absorption spectra of single-crystal graphite at various polarization angle α between the surface normal and the Poynting vector of the light. Short lines at the bottom of the figure are lines denote the peak energies: dashed lines represent the states of π^* symmetry, while solid lines represent the states of σ^* symmetry. States whose symmetry could not be determined are represented by dashed dotted lines. The monochromatic photon energy calibration is estimated to be accurate to ± 0.5eV. (reproduced from Fig. 1 of Ref. [8]), (b) calculated XAS spectra of graphene. The dashed line shows the π^* symmetry and the solid line shows the σ^* symmetry.

is the free electron like energy dispersion. If we integrate the $|M(\vec{k'}, \vec{k})|^2$ along the equi energy contour line in the k space, energy dependent matrix element, $|M(E)|^2$ as in Eq. (2.115), can be calculated which is shown Fig. 3-15(b). Fig. 3-15(b) shows that the $|M(E)|^2$ is increases with increasing energy and $|M(E)|^2$ has maximum value around 293eV and then again smoothly decrease with increasing energy which is a free electron DOS behavior.

Fig. 3-15: figure/mtxpln1.pdf

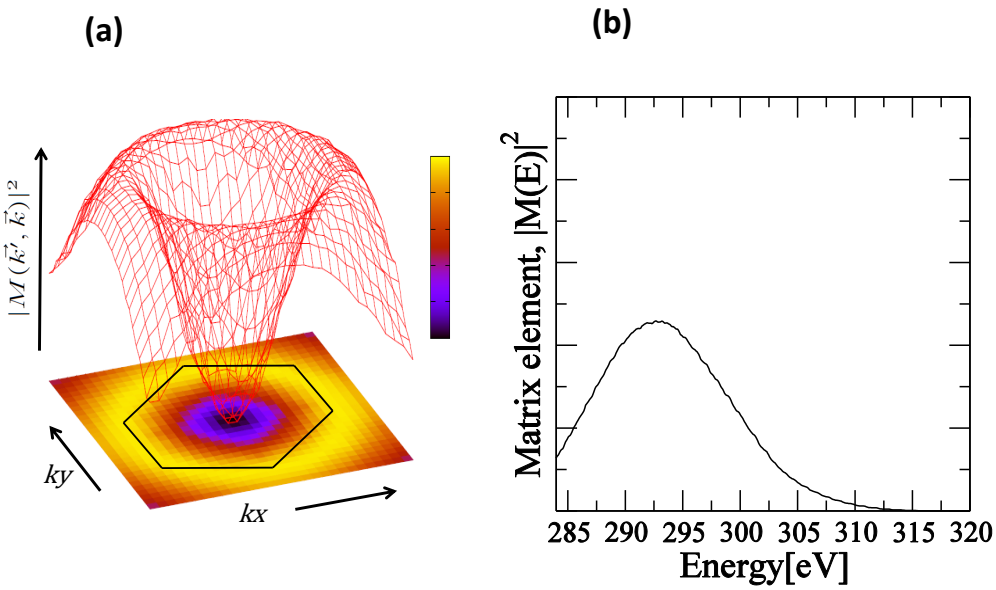

Figure 3-15: (a) Square of $M(\vec{k}', \vec{k})$ as a function of the final wave vector $\vec{k}$ at $\vec{G} = 0$ in the reciprocal space. $\vec{G}$ is the reciprocal lattice vector and (b) Square of M(E) as a function of incident X-ray energy.

Chapter 4

Summary

We have calculated the X-ray absorption spectra of graphene using so called dipole approximation. Transition from the intial 1s energy band to unoccupied π^* and σ^* band are non-vertical transitions because of the large X-ray photon energy and momentum. The intial and the final states can be either in the same atomic site (on-site) or between the nearest neighbor atomic site (off-site). The atomic matrix elements for both on-site and off-site interaction are calculated analytically. The X-ray absorption is dominated by the on-site transition of electron beccause of the strong overlapping of 1s and 2p electron wave functions. It is found that each transition in the X-ray absorption has its own dipole vector and it is oriented in a certain direction which is obtained from the atomic dipole vector. In case of 1s to π^* transition, the dipole vector directed in the z direction, that is perpendicular to the graphene plane, while in 1s to σ^* transition, the dipole vector is directed along the graphene plane. Such different orientation of dipole vectors depending on the final state symmetry gives rise to polarization dependence of X-ray absorption spectra of graphene which is different for 1s-π^* and 1-σ^* transition. The X-ray absorption intensity is proportional to the absorption matrix element which corresponds to the the inner product of dipole vector and polarization vector. Due to the square of the matrix element the X-ray absoption intensity for 1s to π^* linearly proportional to the $\sin^2\alpha$ while for 1s to σ^* the absorption intensity is proportional to the $\cos^2\alpha$. The 1s to π^* (σ^*) absoprtion intensity increases (decreases) with incresing α. Core electron excitation to the higher

unoccupied energy bands can be tackeled if we consider the final state as summation of the plane waves. We derived an analytical expression for absorption probabilty for plane waves as final sate. As a first step, however we only consider the case that the reciprocal translation vector is zero ($\vec{G} = 0$). We have calculated absoprtion intensity which is proportional to the square of the absorption matrix element in the reciprocal space. The energy dependent square of the matrix element resembles density of state of free electron. We are expecting that this will give us more information about the XAS spectra at high energy region.

Bibliography

[1] R. Saito, G. Dresselhaus, and M. S. Dresselhaus, *Physical Properties of Carbon Nanotubes*, Imperial College Press, London, 1998.

[2] P. R. Wallace, Phys. Rev. **71**, 622 (1947).

[3] K. S. Novoselov et al., Science **306**, 666 (2004).

[4] K. S. Novoselov et al., Nature **438**, 197 (2005).

[5] Y. Zhang, Y.-W. Tan, H. L. Stormer, and P. Kim, Nature **438**, 201 (2005).

[6] S. V. Morozov et al., Phys. Rev. Lett. **100**, 016602 (2008).

[7] R. R. Nair et al., Science **320**, 1308 (2008).

[8] R. A. Rosenberg, P. J. Love, and V. Rehn, Phys. Rev. B **33**, 4034 (1986).

[9] S. Y. Zhou et al., Phys. Rev. B **80**, 121409 (2009).

[10] D. Pacilé et al., Phys. Rev. Lett. **101**, 066806 (2008).

[11] A. Grüneis et al., Phys. Rev. B **67**, 165402 (2003).

[12] R. Saito et al., Optical absorption of graphite and single-wall carbon nanotubes, 2004-05-01.

[13] A. Grüneis, *Resonance Raman spectroscopy of single wall carbon nanotubes*, PhD thesis, Tohoku University, 2004.

[14] L. G. Johnson and G. Dresselhaus, Phys. Rev. B **7**, 2275 (1973).

[15] A. G. Marinopoulos, L. Reining, A. Rubio, and V. Olevano, Phys. Rev. B **69**, 245419 (2004).

[16] D. A. Fischer, R. M. Wentzcovitch, R. G. Carr, A. Continenza, and A. J. Freeman, Phys. Rev. B **44**, 1427 (1991).

[17] P. E. Batson, Phys. Rev. B **48**, 2608 (1993).

[18] P. Skytt et al., Phys. Rev. B **50**, 10457 (1994).

[19] W. Hua, B. Gao, S. Li, H. Ågren, and Y. Luo, Phys. Rev. B **82**, 155433 (2010).

[20] P. Castrucci, M. Scarselli, M. De Crescenzi, M. A. El Khakani, and F. Rosei, Nanoscale **2**, 1611 (2010).

[21] M. D. Crescenzi and G. Chiarello, Extended energy loss fine structure measurement above shallow and deep core levels of 3d transition metals, 1985.

[22] A. Damascelli, Z. Hussain, and Z.-X. Shen, Rev. Mod. Phys. **75**, 473 (2003).

[23] A. Bostwick, T. Ohta, T. Seyller, K. Horn, and E. Rotenberg, Nat Phys **3**, 36 (2007).

[24] E. L. Shirley, L. J. Terminello, A. Santoni, and F. J. Himpsel, Phys. Rev. B **51**, 13614 (1995).

[25] R. Saito, G. Dresselhaus, and M. S. Dresselhaus, Phys. Rev. B **61**, 2981 (2000).